iScience

CellPress
OPEN ACCESS

Article

The *CIt* protocol: A blueprint to potentiate the immunogenicity of immunoproteasome-reprogrammed mesenchymal stromal cells

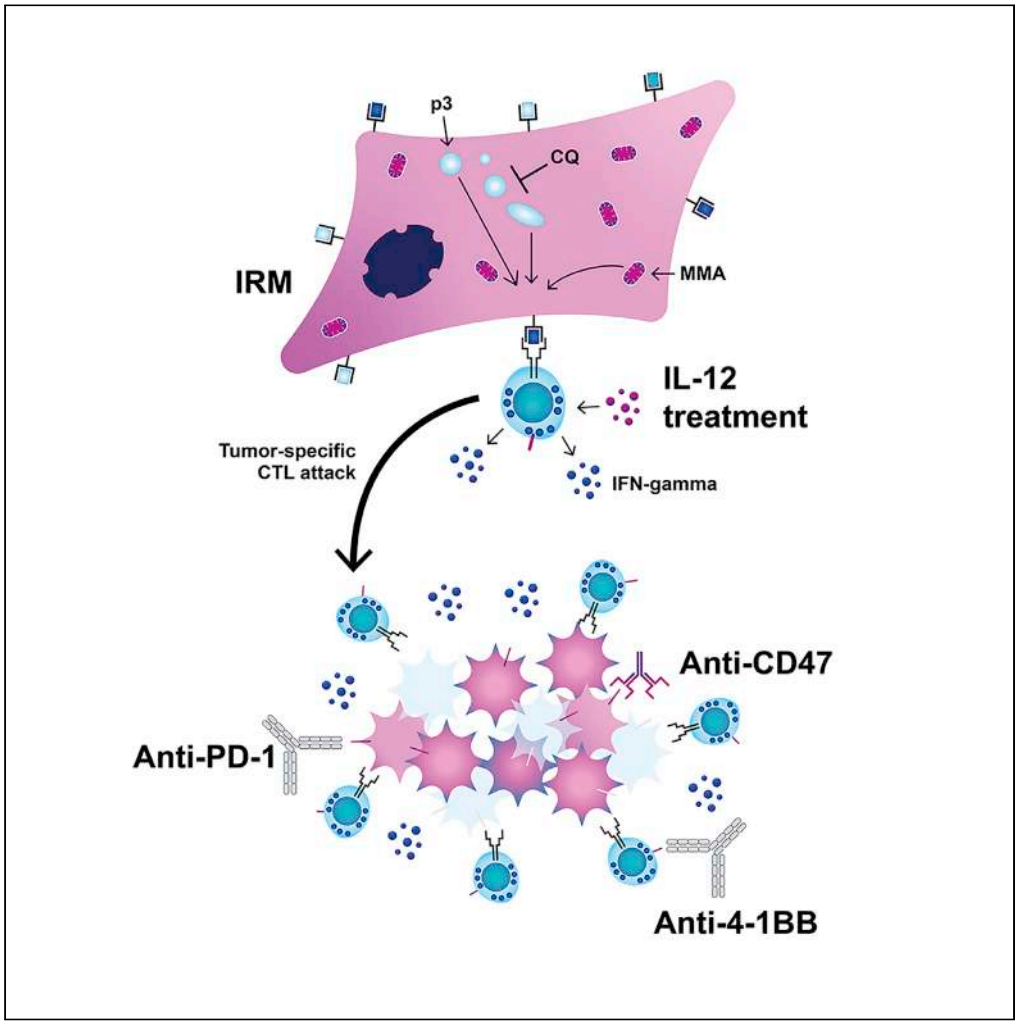

Jean-Pierre Bikorimana, Nehme El-Hachem, Jamilah Abusarah, Nicoletta Eliopoulos, Sebastien Talbot, Riam Shammaa, Moutih Rafei

moutih.rafei.1@umontreal.ca

Highlights

Immunoproteasome-reprogrammed mesenchymal stromal cells (IRMs) are efficient APCs

As anti-cancer vaccine, IRMs lead to significant protective and therapeutic outcomes

The optimized *CtI* protocol provides superior therapeutic effect over IRM monotherapy

Therapeutic antibody-*CtI* protocol combination can unveil unsung synergistic effects

Bikorimana et al., iScience *25*, 105537
December 22, 2022 © 2022 The Author(s).
https://doi.org/10.1016/j.isci.2022.105537

iScience

CellPress
OPEN ACCESS

Article

The *CIt* protocol: A blueprint to potentiate the immunogenicity of immunoproteasome-reprogrammed mesenchymal stromal cells

Jean-Pierre Bikorimana,[1] Nehme El-Hachem,[2,3] Jamilah Abusarah,[2] Nicoletta Eliopoulos,[4,5] Sebastien Talbot,[6] Riam Shammaa,[7] and Moutih Rafei[1,2,8,9,*]

SUMMARY

Immunoproteasome-reprogrammed mesenchymal stromal cells (IRMs) can surpass dendritic cells at eliciting tumor-specific immunity. However, the current IRM vaccination regimen remains clinically unsuitable due to the relatively high dose of IRMs needed. Since the administration of a lower IRM dose triggers a feeble anti-tumoral response, we aimed to combine this vaccination regimen with different modalities to fine-tune the potency of the vaccine. In a nutshell, we found that the co-administration of IRMs and interleukin-12 accentuates the anti-tumoral response, whereas the cross-presentation potency of IRMs is enhanced via intracellular succinate build-up, delayed endosomal maturation, and increased endosome-to-cytosol plasticity. Stimulating phagocyte-mediated cancer efferocytosis by blocking the CD47-SIRPα axis was also found to enhance IRM vaccine outcomes. Upon designing a single protocol combining the above-mentioned strategies, 60% of treated animals exhibited a complete response. Altogether, this is the first IRM-based vaccination study, optimized to simultaneously target three vaccine-related pitfalls: T-cell response, antigen cross-presentation, and cancer phagocytosis.

INTRODUCTION

The search for new cancer vaccines highlights the essential role of cellular responses in targeting and directly killing cancerous cells for the eradication of established tumors.[1–3] The major divergence between cancer vaccines and the ones targeting infectious agents lays in the nature of the targeted antigen (e.g., self vs. non-self, respectively).[1–3] Therefore, a cancer vaccine is challenging to develop due to obstacles related to the identification of tumor-specific antigens (TSAs) capable of generating specific, effective and persistent cytotoxic T lymphocytes (CTLs) without breaking tolerance.[2–7] Although substantial advances in the search for TSAs were made, the techniques currently used for their discovery require extensive and tedious high-throughput and next-generation sequencing protocols given the relative specificity of these TSAs to each patient, rendering this approach relatively impractical. Therefore, a more plausible alternative is to promote antigen cross-presentation of exogenous soluble antigens derived from patient-specific tumors via major histocompatibility complex (MHC)I, a process normally performed by professional antigen-presenting cells (APCs) such as dendritic cells (DCs). Although endogenous DCs remain the most efficient naturally occurring APCs, *ex vivo*-generated monocyte-derived DCs, which are commonly used in the clinic, exhibit suboptimal antigen cross-presentation amongst many other limitations, which explains their clinical failure.[8] By focusing on DCs to achieve better CTL activation, researchers identified a promising $CD141^{+}XCR1^{+}$ DC subset in humans harboring exceptional cross-presentation properties.[9,10] However, the scarcity of these cross-presenting DCs makes it unsuitable for the design of optimal vaccine doses.[9,10] Therefore, establishing a decent supply of an APC capable of bypassing some of the DC-related limitations remains a central goal in the field.

In concordance with the efforts focusing on overcoming the shortcomings of DCs, we recently engineered a new cellular vaccine by expressing the immunoproteasome (IPr) complex in mesenchymal stromal cells (MSCs).[11] Not only can these IPr-reprogrammed MSCs (IRMs, previously named MSC-IPr) behave as stable APCs, compared to interferon (IFN)-gamma-stimulated MSCs, but their capacity to activate CTLs surpasses

[1]Department of Microbiology, Infectious Diseases and Immunology, Université de Montréal, Montreal, QC, Canada

[2]Department of Pharmacology and Physiology, Université de Montréal, Montreal, QC, Canada

[3]Pediatric Hematology-Oncology Division, Centre Hospitalier Universitaire Sainte-Justine Research Centre, Montreal, QC, Canada

[4]Lady Davis Institute for Medical Research, Jewish General Hospital, Montreal, QC, Canada

[5]Department of Surgery, McGill University, Montreal, QC, Canada

[6]Department of Biomedical and Molecular Sciences, Queen's University, Kingston, ON, Canada

[7]IntelliStem Technologies Inc., Toronto, ON, Canada

[8]Molecular Biology Program, Université de Montréal, Montreal, QC, Canada

[9]Lead contact

*Correspondence: moutih.rafei.1@umontreal.ca

https://doi.org/10.1016/j.isci.2022.105537

This is an open access article under the CC BY-NC-ND license (http://creativecommons.org/licenses/by-nc-nd/4.0/).

those of monocyte-derived DCs.[11] Although highly efficient at eradicating established lymphoma and melanoma tumors when combined with the anti-PD-1 immune-checkpoint blocker and the anti-4-1BB agonist antibody, scalability issues remain a crucial barrier for their translational use in the clinic.[11] For instance, all efficacy studies conducted in pre-clinical models used a large cell dose (10^6 cells/dose/20g of weight), which translates to more than 3 billion cells/dose for a single 70 kg patient. Thus, optimization studies are warranted to maximize IRMs' potency and to bring forward practical vaccination protocols.

By testing several cellular doses and comparing delivery routes, we found that the subcutaneous (SC) delivery of a dose as low as 5×10^3 IRMs /mouse can trigger marginal anti-tumoral responses in mice. Starting from that point, we investigated various strategies targeting effector **C**TLs, **I**RM-mediated antigen processing, and the **t**umor itself to finally establish the *CIt* protocol, a vaccination regimen easily adaptable to clinical settings.

RESULTS

Immunoproteasome-reprogrammed mesenchymal stromal cells are transcriptionally similar to dendritic cells than innate mesenchymal stromal cells

The initial rationale behind the development of IRMs (previously referred to as MSC-IPr, now branded as IRMs to dissociate them from the suppressive "world" of innate MSCs) was to come-up with a possible alternative and/or complementary tool to the commonly used monocyte-derived DCs as a mean to prime potent anti-tumor CTLs. We thus sought to compare the molecular signature of their antigen presentation capacity with DCs and innate MSCs in order to identify similar and/or divergent gene expression profiles. Using transcriptomic data, we first assessed the extent to which IRMs and DCs share similar gene signatures compared to innate MSCs (Figure 1A). Our combined analysis detected 468 down- and 521 up-regulated genes at the given significance threshold (see STAR Methods section), which overlapped between IRMs and DCs versus innate MSCs (Figure S1). For instance, gene set enrichment analysis (GSEA) identified the gene ontology (GO) biological process of antigen presentation by MHCI to be enriched at the top of the list for IRMs versus innate MSCs (top panel; ES = +0.48, *q*-value = 0.01) and for DCs versus innate MSCs (lower panel; ES = +0.55, *q*-value = 0.0035), respectively (Figure 1B). The log2 fold change of genes associated with MHCI-based antigen presentation showed a better concordance between IRMs and DCs (Figure 1C lower panel; spearman rho = 0.21 when considering all differentially expressed genes in IRMs and DCs; and spearman rho= 0.54 p-value = 4.3e-6 for MHCI-based antigen presentation process GO:0042590) compared to the background of all sequenced genes (Figure 1C upper panel). Importantly, we performed clustering of significant gene expression patterns from the GO: MHCI in the euclidean space (Figure 1D) and found IRMs to be transcriptionally similar to DCs as opposed to innate MSCs. Since MHCI genes could be ubiquitously expressed, we further established a more holistic approach by scoring the top 250 up- and 250 down-regulated genes, from the DCs versus innate MSCs contrast, against the ranked list of differentially expressed genes in IRMs. The combined enrichment score (ES = +0.48; p-value < 0.001) strongly suggests that both DCs and IRMs share similar transcriptional regulators (Figure S2). We also found that commonly up-regulated genes are enriched for several immune-related GO Biological processes (cytokine production, antigen processing, innate and adaptive immunity - Figure S3).

The subcutaneous delivery of low-dose immunoproteasome-reprogrammed mesenchymal stromal cells remains therapeutically active

The IRM vaccine was previously shown to elicit powerful anti-tumoral responses leading to the regression of established T-cell lymphoma and melanoma when combined with anti-PD-1 and anti-4-1BB targeting antibodies.[11] However, the vaccine was delivered via the intraperitoneal (IP) route, which is not commonly used in the clinic.[12–15] Second, all vaccinated animals received a dose of 10^6 cells per injection (~20g mouse), which translates to 3.5×10^7 cells for a 70 kg subject. Since such doses are logistically and practically difficult to achieve especially at larger scales, we next wondered if a lower IRM dose can still elicit a therapeutic response under prophylactic settings. For this purpose, we conducted a vaccine dosing study in syngeneic C57BL/6 mice while comparing the IP and SC routes (Figure S4A). Although a dose-dependent therapeutic effect was observed with both routes, animals receiving the lowest dose (5×10^3 cells) showed a slight delay in death with IP delivery (Figure S4B) in contrast to a 20% survival achieved using the SC route (Figure S4C). The sum of these data highlights two important conclusions. First, it indicates

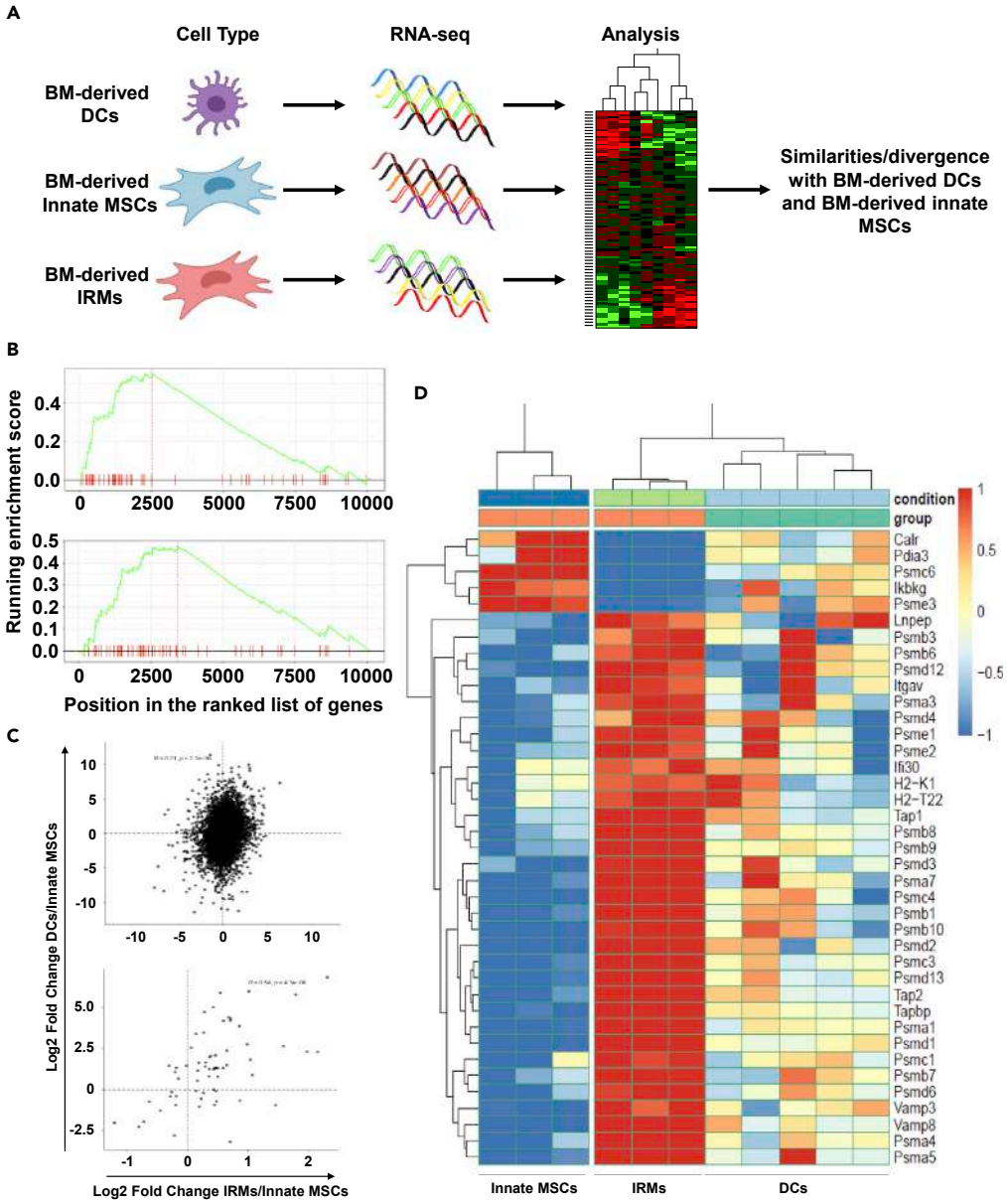

Figure 1. Comparing the molecular signature of IRMs to BM-derived DCs

(A) Schematic diagram of the workflow used in this study. DC-related transcriptomic dataset was used from GEO (accession: GSE158783).

(B) The plot illustrates the running enrichment scores from GSEA. Upper panel: cumulative enrichment score of MHCI genes from GO biological process in DCs vs control (innate) MSCs. Lower panel: same as the upper panel but presenting IRM/Control comparison.

(C) The scatter plot represents pairwise log2 fold change correlations across settings. Top panel: spearman's rank correlation considering all genes. Lower panel: spearman's rank correlation for the MHCI (GO:0042590).

(D) A heatmap showing euclidean-based clustering. Columns are samples from the 3 conditions (controls, IRMs and BM-derived DCs) and rows are significantly regulated genes (up/down DEGS; FDR < 0.05) and common to both contrasts from panel C. See also Figures S1–S3.

that SC delivery of IRMs is superior to the IP route in eliciting an anti-tumoral response. Second, it demonstrates a marginal, yet important, residual therapeutic effect triggered by the lowest IRM cellular dose (equivalent to 15-20 × 10^6 cells/dose for a 70 kg subject), which represents an opportunity for further improvements to maximize its therapeutic potency.

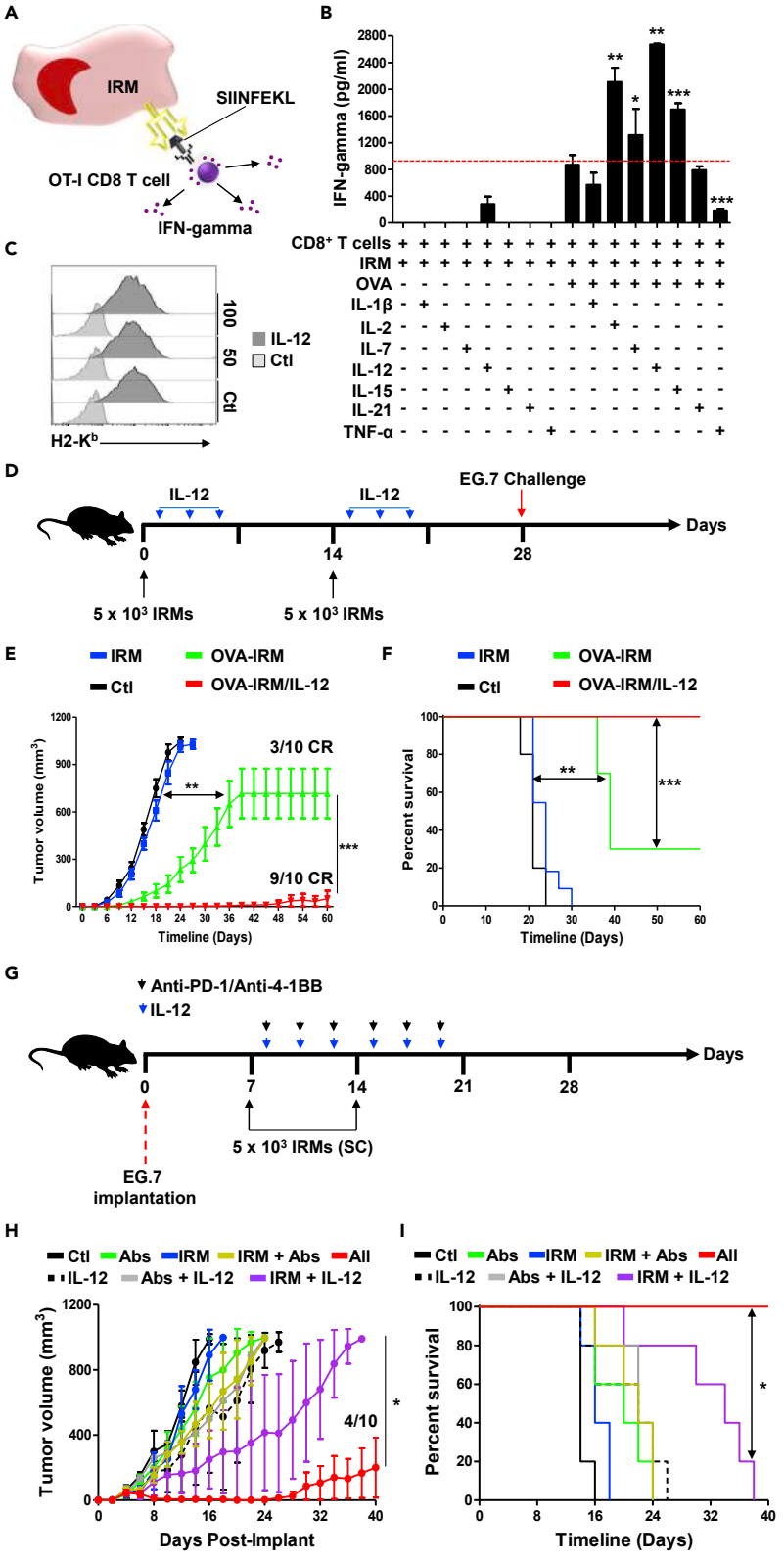
A
IRM
SIINFEKL
OT-I CD8 T cell
IFN-gamma
B
IFN-gamma (pg/ml)
CD8+ T cells
IRM
OVA
IL-1β
IL-2
IL-7
IL-12
IL-15
IL-21
TNF-α
C
IL-12
Ctl
H2-Kb
D
IL-12
IL-12
EG.7 Challenge
Days
5 x 10³ IRMs
5 x 10³ IRMs
E
IRM
OVA-IRM
Ctl
OVA-IRM/IL-12
Tumor volume (mm³)
3/10 CR
9/10 CR
Timeline (Days)
F
IRM
OVA-IRM
Ctl
OVA-IRM/IL-12
Percent survival
Timeline (Days)
G
Anti-PD-1/Anti-4-1BB
IL-12
Days
5 x 10³ IRMs (SC)
EG.7
implantation
H
Ctl
Abs
IRM
IRM + Abs
All
IL-12
Abs + IL-12
IRM + IL-12
Tumor volume (mm³)
4/10
Days Post-Implant
I
Ctl
Abs
IRM
IRM + Abs
All
IL-12
Abs + IL-12
IRM + IL-12
Percent survival
Timeline (Days)

Figure 2. Investigating the effect of IL-12 on IRM-induced anti-tumoral response

(A) Schematic diagram depicting the antigen cross-presentation assay used for cytokine screening.

(B) IFN-gamma quantification by ELISA derived from the antigen presentation assay conducted in the presence of various pro-inflammatory cytokines.

(C) Representative flow-cytometry analysis of H2-K^b on the surface of IRMs in response to different IL-12 doses (50 and 100 ng/mL).

(D) Schematic diagram showing the study design for the prophylactic vaccination.

(E) Tumor growth curve of animals vaccinated using 5 × 10^3 IRMs (blue), OVA-pulsed 5 × 10^3 IRMs (green), and 5 × 10^3 OVA-pulsed IRMs combined with IL-12 administration (red). Non-vaccinated animals receiving the EG.7 tumor cells are shown in black. Complete Response (CR) out of 10 are shown for OVA-pulsed IRMs and OVA-pulsed IRMs plus IL-12.

(F) The Kaplan-Meier survival curve of the experiment shown in panel (E).

(G) Schematic diagram showing the study design for the therapeutic vaccination.

(H) Tumor growth curve of animals with pre-established EG.7 tumors vaccinated using 5 × 10^3 OVA-pulsed IRMs (blue), 5 × 10^3 OVA-pulsed IRMs + anti-PD-1/anti-4-1BB antibodies (Abs) (yellow), 5 × 10^3 OVA-pulsed IRMs + IL-12 (purple), and 5 × 10^3 OVA-pulsed IRMs + anti-PD-1/anti-4-1BB Abs + IL-12 (red). Non-vaccinated control mice are shown in black, Abs only treatment in green, IL-12 only in black dotted line, and Abs combined with IL-12 in gray.

(I) The Kaplan-Meier survival curve of the experiment shown in panel (E). For panel B, n = 6/group. For panels E-F and H-I, n = 10/group. Results are represented as means with S.D. error bars, and statistical significance is represented with asterisks: *P<0.05, **P<0.01, ***P<0.001. See also Figures S4 and S5.

Interleukin (IL)-12 is a major booster of immunoproteasome-reprogrammed mesenchymal stromal cells-induced anti-tumoral response

To elicit a CTL response, APCs must provide three important signals to responding CD8 T cells.[16,17] The first two signals are related to antigen presentation by MHCI and co-stimulation by CD80 and/or CD86. The third signal consists of supporting the proliferation and/or activation of stimulated T cells through cytokine supply.[16,17] We thus questioned whether the addition of various pro-inflammatory cytokines to CD8 T cells co-cultured with antigen-pulsed IRMs could amplify their activation (Figure 2A). We selected the best-acting γc-cytokines (IL-2, IL-7, IL-15, and IL-21) and other pro-inflammatory mediators such as IL-1β, IL-12, and tumor necrosis factor (TNF)-alpha. Although IL-2, IL-7 and IL-15 all enhanced IFN-gamma production by responding OT-I CD8 T cells, the highest T-cell response was reached with IL-12 (Figure 2B). To confirm that the enhanced IL-12-mediated T-cell stimulation did not result from a direct increase in MHCI expression, IRMs were first treated with IL-12 and then assessed for their cell surface expression level of MHCI in response to ascending IL-12 doses, and we detected no changes (Figure 2C). As such, we next designed a prophylactic vaccination experiment using the lowest IRM cell dose (5 × 10^3) combined with an IL-12 regimen delivered during weeks 1 and 3 following the first vaccination (Figure 2D). Interestingly, the IL-12/IRM combination intensified the potency of the vaccine (Figure 2E) with a survival rate of 100% in contrast to 30% with the IRMs only group (Figure 2F). This observation provided the impetus to further test this protocol in a therapeutic setting, which would include the use of anti-PD1 and anti-4-1BB (Figure 2G) as previously reported.[11] Although the vaccination of EG.7 tumor-bearing mice with 5 × 10^3 IRM cells combined with anti-PD1/anti-4-1BB (yellow line) led to moderate delays compared to the higher delays seen with the IRM/IL-12 combo (purple line- Figures 2H, 2I, S5A), 100% of animals remained alive when IRMs, IL-12, and anti-PD1/4-1BB antibodies were administered together (red line - Figures 2H, 2I and S5A). Notably, 40% of treated animals exhibited a complete response (CR) using this combination strategy (Figure S5A). These data clearly indicate that anti-PD-1/4-1BB combined with IRM-induced anti-tumoral immunity can synergize with IL-12 and potentially other powerful pro-inflammatory mediators.

Targeting succinate production or endosomal maturation improves the therapeutic potency of immunoproteasome-reprogrammed mesenchymal stromal cells

We have previously reported that it is indeed possible to pharmacologically enhance or instill the process of antigen cross-/presentation in both IRMs and innate MSCs.[11,18,19] As such, we next investigated whether the antigen cross-presentation ability of IRMs could be pharmacologically enhanced following a mono- or combinatory treatment. For instance, by enhancing the succinate metabolite, production of reactive oxygen species (ROS) can be augmented, which would directly promote the expression of the pro-inflammatory transcription factor hypoxia-inducible factor (HIF)-1α, and, ultimately, pro-inflammatory cytokine production.[20–23] Furthermore, accumulation of succinate can trigger the production of several pro-inflammatory cytokines, including IL-1β, IL-2, IL-12, and IL-18.[20] Thus, intracellular succinate levels can be enhanced in IRMs via treatment with methylmalonic acid (MMA) to block succinate dehydrogenase. Another strategy to pharmacologically enhance the cross-presentation potency of IRMs is to treat them

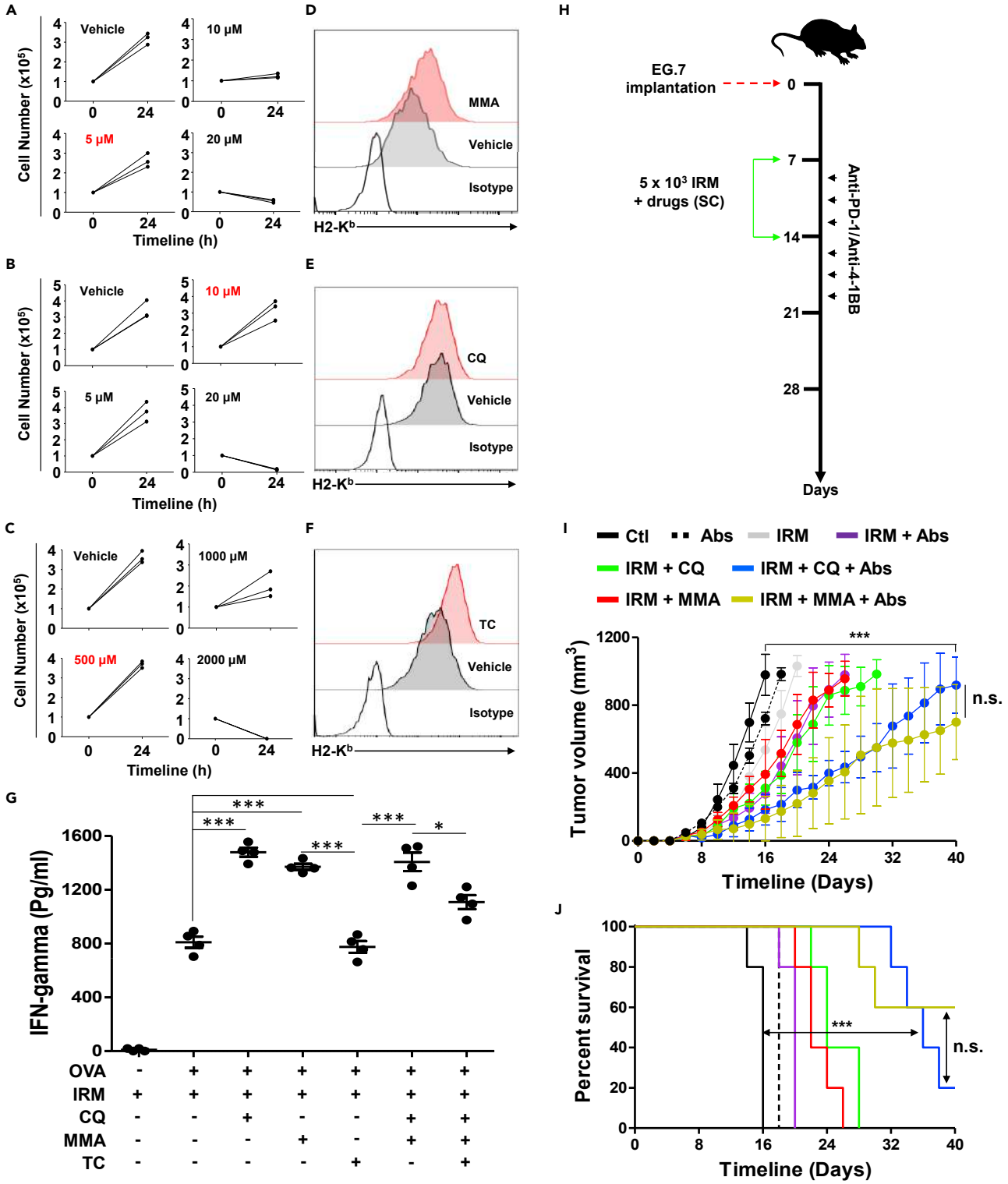

Figure 3. Evaluating the therapeutic potency of pharmacologically enhanced IRMs

(A) Identifying the MTD for MMA on IRMs.

(B) Identifying the MTD for CQ on IRMs.

(C) Identifying the MTD of TC on IRMs.

(D) Representative flow-cytometry analysis of H2-K^b on IRMs in response to MMA treatment.

Figure 3. *Continued*

(E) Representative flow-cytometry analysis of H2-K^b on IRMs in response to CQ treatment.

(F) Representative flow-cytometry analysis of H2-K^b on IRMs in response to TC treatment.

(G) IFN-gamma quantification by ELISA derived from the antigen presentation assay conducted using pharmacologically enhanced IRMs.

(H) Schematic diagram showing the study design for the therapeutic vaccination.

(I) Tumor growth curve of animals vaccinated using 5 × 10^3 OVA-pulsed IRMs (gray), 5 × 10^3 IRMs + Abs (purple), 5 × 10^3 OVA-pulsed CQ-treated IRMs (green), 5 × 10^3 OVA-pulsed MMA-treated IRMs (red), 5 × 10^3 OVA-pulsed CQ-treated IRMs + Abs (blue), and 5 × 10^3 OVA-pulsed MMA-treated IRMs + Abs (yellow). Non-vaccinated animals receiving the EG.7 tumor cells are shown in black whereas animals receiving the Abs only treatment are shown in the dotted black line.

(J) The Kaplan-Meier survival curve of the experiment shown in panel (I). For panels A-C, n = 3/group. For panel G, n = 4/group. For panels I-J, n = 10/group. Results are represented as means with S.D. error bars, and statistical significance is represented with asterisks: *P<0.05, **P<0.01, ***P<0.001.

with chloroquine (CQ) to delay endosomal maturation and limit endo-lysosomal-mediated degradation of internalized antigens.[11] Our third pharmacological approach would consist of treating IRMs with tranylcypromine (TC), a drug capable of specifically inhibiting the lysine-specific histone demethylase 1 (LSD1) complex to ensure an effective increase and/or stabilization of MHCI cell surface levels.[18] Following the identification of the maximum tolerated dose (MTD) for each of the three compounds (Figures 3A–3C), flow-cytometry assessment of IRMs revealed a substantial increase of cell surface H2-K^b in response to MMA and TC (Figures 3D and 3F). Surprisingly, however, only MMA and CQ enhanced the responsiveness of co-cultured OT-I T cells with no detectable effect observed with TC treatment (Figure 3G) despite its induced H2-K^b increase observed earlier (Figure 3F). Furthermore, the combination of all three drugs led to lower T-cell activation compared to MMA and/or CQ treatments suggesting a potential competing/negative effect mediated by TC when added to the mix (Figure 3G). These results led us to next test these pharmacologically stimulated IRMs in the context of therapeutic vaccination against EG.7 T-cell lymphoma (Figure 3H). Although an overall delay in tumor growth was observed in all IRM-treated groups, the effect was more pronounced with CQ- or MMA-treated IRMs combined with anti-PD-1/4-1BB (Figures 3I and 3J). These data clearly indicate that targeting succinate production (using MMA) or delaying endosomal maturation (using CQ) can enhance the potency of IRMs, but only when combined with anti-PD-1 and anti-4-1BB targeting antibodies.

Stimulating endosome-to-cytosol release enhances immunoproteasome-reprogrammed mesenchymal stromal cells-induced immunity

The entrapment of captured biomolecules in the endosomal compartment is a major deterrent to the efficacy of various therapeutic modalities including cellular vaccines.[24,25] This led us to speculate that breaking endosomal membranes to release captured proteins could further promote antigen cross-presentation and T-cell activation. To validate this hypothesis, we used an endo-osmolytic peptide derived from the membrane-lytic spider venom M-lycotoxin (Figure 4A).[26] Of the three tested peptide sequences (Figure 4B), p3 led to the strongest T-cell response (Figures 4B and 4C). We next used two different assays to confirm that p3 triggers indeed endosomal escape. The first assay consists of pulsing IRMs with the cytoplasmic dye coumarin-cephalosporin-fluorescein (4)-acetoxymethyl (CCF4-AM) and recombinant β-lactamase.[27] If the endosomal membranes are damaged, recombinant β-lactamase diffuses to the cytoplasm and cleaves CCF4-AM triggering an alternative Fluorescence Resonance Energy Transfer (FRET) signal (Figure 4D), which was indeed detected by flow cytometry in p3-treated IRMs (Figure 4E). The second assay follows the same concept except that it uses recombinant cytochrome (rCyt)-C as a mean to trigger apoptosis. In other words, when rCyt-C is captured, it is entrapped within endosomes unless released through the action of p3, consequently triggering cell death by apoptosis as shown in our analysis (Figures 4F and 4G). Another salient observation of p3 is its capacity to increase both antigen capture (Figures 4H and 4I) and internal processing (Figures 4J and 4K). The sum of these p3-mediated effects correlates with an improved therapeutic potency observed in mice with pre-established EG.7 tumors (blue line - Figures 4L and 4M). We can thus claim that stimulating endosome-to-cytosol release of captured proteins is beneficial to the anti-tumoral activity of IRMs.

Blocking the CD47-SIRPα axis enhances immunoproteasome-reprogrammed mesenchymal stromal cells-induced immunity

The modulatory function of MSCs is commonly attributed to their immune-suppressive secreatome.[28–31] However, two recent reports provided clear evidence that MSC-induced immune-suppression is mediated by endogenous phagocytes following efferocytosis of infused MSCs.[32,33] Although this efferocytosis process is believed to be mainly driven by cell surface phosphatidylserine, MSCs and IRMs can also express

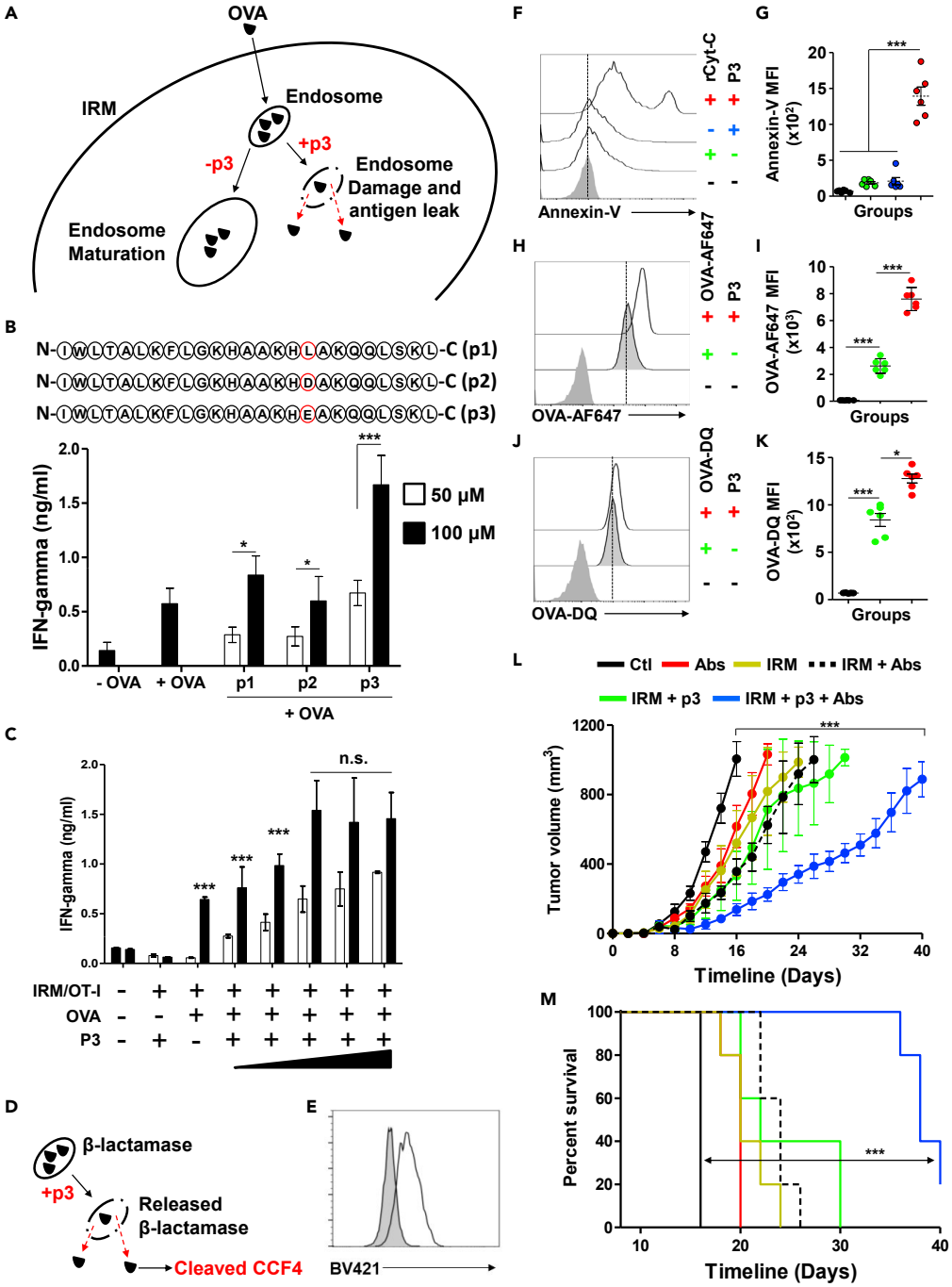

Figure 4. Eliciting endosomal leakage in IRMs enhances their anti-tumoral immunity

(A) Schematic diagram of the mode of action of the used cationic peptide.

(B) The sequences of all three tested cationic peptides and their impact on antigen cross-presentation by IRMs at two different concentrations.

(C) Antigen presentation assay conducted using p3-treated IRMs. The doses tested are: 17.5, 50, 100, 150, and 200 µM. The black bars represent the antigen presentation assay supplemented with the p3 peptide. White bars represent the same condition without the p3 peptide.

(D) Schematic diagram of the CCF4-based assay.

(E) Flow-cytometry analysis of β-lactamase/CCF4-pulsed IRMs in the presence (white histogram) or absence (gray histogram) of p3.

(F) Flow-cytometry analysis of apoptosis induced in IRMs following rCyt-C and p3 treatment.

Figure 4. *Continued*

(G) The MFI of the signal presented in panel (F).

(H) Flow-cytometry analysis of OVA-AF647 capture by IRMs following p3 treatment.

(I) The MFI of the signal presented in panel (H).

(J) Flow-cytometry analysis of OVA-DQ processing by IRMs following p3 treatment.

(K) The MFI of the signal presented in panel (J).

(L) Tumor growth curve of animals vaccinated using 5×10^3 OVA-pulsed IRMs (yellow), 5×10^3 IRMs + Abs (black dotted line), 5×10^3 OVA-pulsed IRMs + p3 (green), and 5×10^3 OVA-pulsed IRMs + p3 + Abs (blue). Non-vaccinated animals receiving the EG.7 tumor cells are shown in black whereas animals receiving the Abs treatment only are shown in red.

(M) The Kaplan-Meier survival curve of the experiment shown in panel (L). For panels L-M, n = 10/group. Results are represented as means with S.D. error bars, and statistical significance is represented with asterisks: *P<0.05, **P<0.01, ***P<0.001.

counter-acting "don't eat me" signals such as CD47, which can quench efferocytosis by binding to signal regulatory protein alpha (SIRPα) on the surface of myeloid cells.[34] We thus exploited this approach to transfer all IRM-containing immunogenic peptides/antigens to resident phagocytes as a mean to ensure effective T-cell stimulation in case infused IRMs fail to survive long enough to prime a CTL response. As expected, pre-treating IRMs with anti-CD47 antibodies prior to their infusion (Figure 5A) impacts anti-tumoral immunity (red versus blue lines - Figures 5B and 5C). Besides, CD47 was also strongly expressed on the surface of EG.7 tumor cells (Figure 5D). This is particularly important as CD47 neutralization is central to enhance cancer cell efferocytosis by resident phagocytes (Figure 5E).[35–41] This begs the question: can anti-CD47 antibody co-administration improve the therapeutic potency of the IRM vaccine? When tested in a therapeutic vaccination study (Figure 5F), the IRM/anti-CD47 combo was found to delay tumor growth, but to a weaker extent compared to the group receiving in addition the anti-PD-1 and anti-4-1BB (green versus red lines - Figure 5G). In fact, all mice in the IRM/anti-CD47 group died by day 36 in contrast to a 40% survival rate when combined with anti-PD-1/4-1BB (Figure 5H). These data not only provide a new possible combo for IRM-based vaccination but also highlight an important role for the CD47-SIRPα axis during antigen presentation.

Combining all tested strategies annihilates tumor growth

We have tested so far multiple combination strategies in our pursuit of a vaccination protocol capable of eradicating tumors using low-dose IRMs. Consistent with this idea, we next conducted an antigen-presentation assay combining these pharmacological treatments. Although IL-12 combined with MMA or CQ leads to similar T-cell activation outcomes, these co-treatments were stronger than the IL-12/p3 combo (Figure 6A). Nevertheless, the highest T-cell activation response was observed when MMA, CQ, p3, and IL-12 were all combined (Figure 6A). To validate the potency of this combination *in vivo*, we designed a study where EG.7 tumor-bearing mice first received the anti-CD47 antibody followed by low-dose pharmacologically stimulated IRMs along with anti-PD-1/4-1BB and IL-12 (Figure 6B). This protocol revealed that pharmacologically enhanced IRMs delivered alone result in the same tumor growth delay as treatment with all three antibodies (anti-CD47, anti-PD-1, and anti-4-1BB) delivered with IL-12 (Figure 6C). Remarkably, pharmacologically enhanced IRMs combined with IL-12 and all three antibodies controlled tumor growth in all mice with a 100% survival rate and 60% CR reached by the end of the experiment (Figures 6C, 6D, and S5B). Thus, low-dose IRMs can be effectively used as part of a multifactorial vaccination protocol targeting endogenous CTLs (anti-PD-1/4-1BB and IL-12), IRMs (MMA, CQ, and p3), and tumor cells (anti-PD-1 and anti-CD47).

DISCUSSION

The development of DC-based vaccines capable of eliciting tumor-specific CTLs remains a central goal for controlling pre-established tumors. Despite significant improvements, clinical responses to DC vaccines remain largely frail due to hurdles related to insufficient antigen cross-presentation, impaired migratory capacity, and/or weak cytokine release.[42–48] With these limitations in perspective, we engineered IRMs, a type of non-hematopoietic APCs capable of surpassing DCs at mounting potent anti-tumoral responses against both murine T-cell lymphoma and melanoma caused by EG.7 and B16 cells, respectively.[11] Although exhibiting impressive potencies in pre-clinical models, the IRM vaccination protocol used so far is logistically impractical. We thus tested different therapeutic modalities targeting **C**TLs activation, **I**RMs function, and the **t**umor itself to establish the *CIt* protocol.

Pro-inflammatory cytokines play central roles in defining and/or amplifying induced CTL responses,[17] which is why we thought of combining them with low-dose IRM vaccination. In fact, multiple DC vaccines

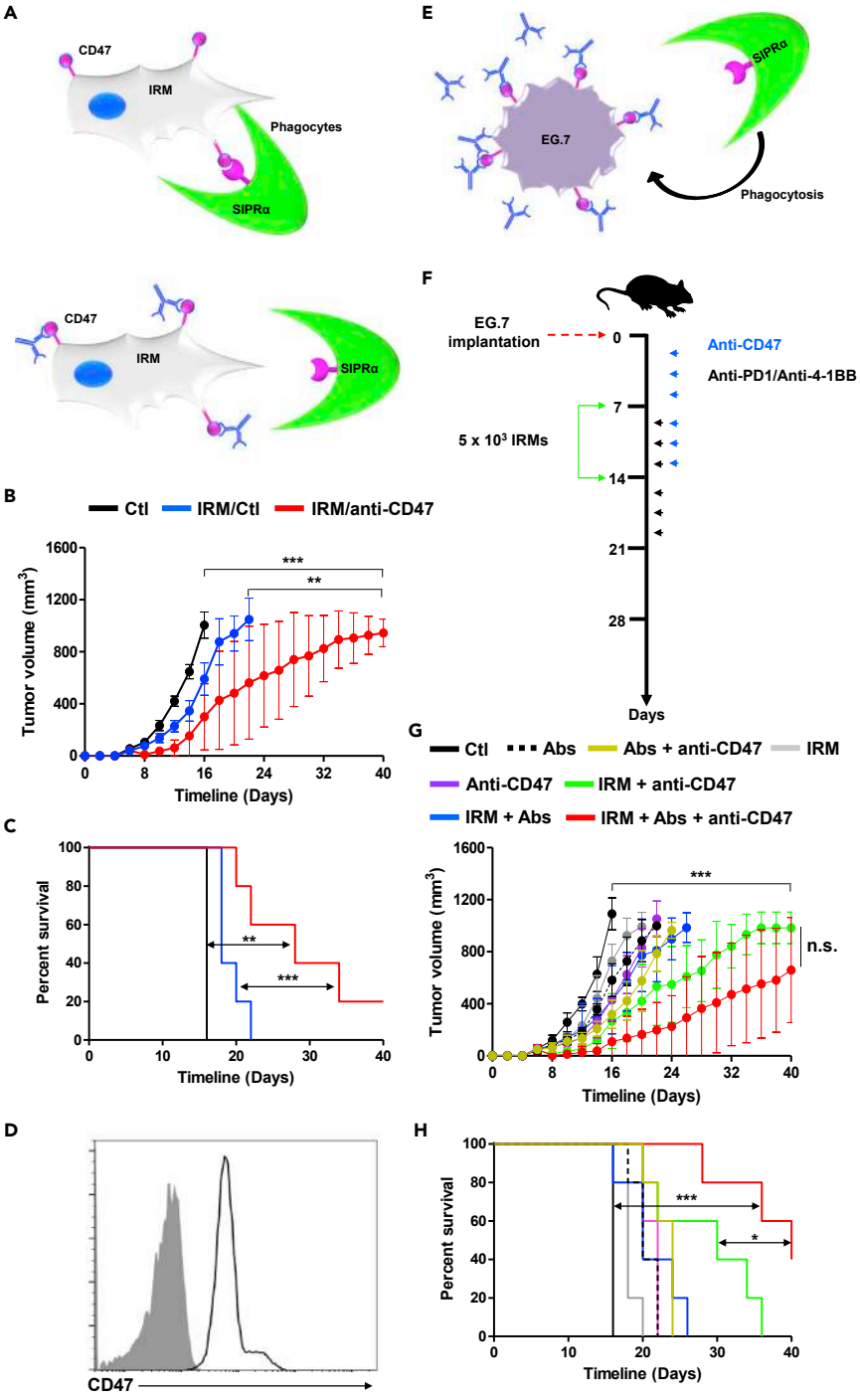

Figure 5. Enhancing efferocytosis through CD47 neutralization is beneficial to IRMs activity

(A) Schematic diagram depicting the rationale for using anti-CD47 directly on IRMs.

(B) Tumor growth curve of animals vaccinated using 5 × 10^3 OVA-pulsed IRMs pre-treated with isotype control (blue), and 5 × 10^3 OVA-pulsed IRMs pre-treated with anti-CD47 (red). Non-vaccinated animals receiving the EG.7 tumor cells are shown in black.

(C) The Kaplan-Meier survival curve of the experiment shown in panel (B).

(D) Representative flow-cytometry analysis of CD47 on the surface of EG.7 tumors.

(E) Schematic diagram depicting the rationale for co-delivery of anti-CD47 with IRMs.

(F) Schematic diagram showing the study design for the therapeutic vaccination combining anti-CD47.

Figure 5. *Continued*

(G) Tumor growth curve of animals vaccinated using 5 × 10^3 OVA-pulsed IRMs (gray), 5 × 10^3 IRMs + anti-CD47 (green), 5 × 10^3 OVA-pulsed IRMs + Abs (blue), and 5 × 10^3 OVA-pulsed IRMs + all Abs (red). Non-vaccinated animals receiving the EG.7 tumor cells are shown in black, Abs only treatment in dotted black line, anti-CD47 only treatment in purple, and all Abs combined in yellow.

(H) The Kaplan-Meier survival curve of the experiment shown in panel (G). For panels B, C, G, and H, n = 10/group. Results are represented as means with S.D. error bars, and statistical significance is represented with asterisks: *P<0.05, **P<0.01, ***P<0.001.

were previously delivered in combination with IL-2, IL-18, or granulocyte-macrophage colony-stimulating factor.[49–52] Antigen cross-presentation was even improved using *ex vivo* FMS-like tyrosine kinase 3 ligand-differentiated DCs[53] More importantly, cross-presenting human CD141+ dendritic cells (cDC1) were reported to promote type 1 immune responses through intrinsic IL-12 secretion.[54] This perfectly correlates with the pronounced anti-tumoral effects we observed when the IRM/antibody combo is co-delivered with IL-12. Notably, the enhanced *in vitro* T-cell activation observed using both IL-7 and IL-15 suggests that combing both of these two cytokines with IRM vaccination may not only lead to potent anti-tumoral responses, but can also trigger a long-term protection given their supportive role in memory development.[55] IL-2, on the other hand, is a strong inducer of CTL proliferation, but the high affinity of this cytokine to the trimeric IL-2 receptor (CD25-CD122-CD132) expressed on the surface of steady state Tregs limits its therapeutic efficacy.[56] This outcome can be bypassed with the use of IL-2 muteins such as NKTR-214 (Nektar Therapeutics), SAR444245 (Sanofi), or NL-201 (Neoleukin), which are specifically engineered to activate NK/naive CD8 T-cells while avoiding Treg stimulation.[57–61] Overall, novel combinations can be designed and tested using various other cytokines, chemokines or even fusokines (the fusion of two unrelated cytokines/chemokines) to mold IRM-elicited immune responses.[62–65]

Regulating protein proteolysis can directly affect antigen cross-presentation.[66] For example, the SNARE protein SEC22B can reduce antigen degradation in DCs by inhibiting the recruitment of lysosomal machinery to endosomes.[67] Likewise, knocking-out the YTHDF1 protein, which normally stimulates the degradation of internalized antigens by promoting the activity of lysosomal cathepsins, enhances DCs' cross-presentation capacity without altering their development, expression of co-stimulatory proteins or cytokine secretion.[68] Given the important role of endosomal activity/function on antigen cross-presentation, we pharmacologically treated IRMs with CQ to delay endosomal maturation to preserve captured OVA from non-specific degradation normally mediated by proteases activated during endosomal maturation.[11] This approach enhanced indeed the potency of IRMs when combined with anti-PD-1 and anti-4-1BB. In line with the same idea, we used the endo-osmolytic p3 to promote endosome-to-cytosol release of the antigen where it can be processed by the proteasomal machinery and found similar beneficial effect on the vaccine response.[26] The rationale for treating IRMs with MMA, on the other hand, was different as this drug, although not known to alter antigen proteolysis, blocks the conversion of succinate to fumarate in the Krebs cycle[20] As a result, succinate builds up and inhibits HIF-1α degradation by the prolyl hydroxylase domain resulting in enhanced cross-presentation and CTL stimulation due to increased expression of H2-K^b/H2-D^b and IL-12 respectively.[11,20] Although the chosen pharmacological treatments highlight a major role for endosomes in antigen cross-presentation, additional studies targeting recycling endosomes or regulating intracellular endosomal trafficking using known or novel compounds identified by high-throughput screening assays may pave the path for additional strategies promoting antigen cross-presentation.[69,70]

Attenuating tumor-driven suppression of T cells represents another viable therapeutic approach for cancer vaccination.[71] For instance, RNAi or CRISPR-Cas9 can both be used to knockdown inhibitory genes in IRMs to reinvigorate exhausted T cells.[71] However, this approach is technically challenging for two main reasons. To start, this strategy can ensure the absence of these immune-checkpoints on the surface of IRMs but will have no impact on their expression on the surface of endogenous responding CTLs. Second, this implies another genetic engineering step, which adds another layer of complexity to IRM generation especially if one envisions the design of this vaccine on a patient-to-patient basis. Thus, the co-administration of the IRM vaccine with different antibodies targeting one or multiple checkpoints represents a more plausible alternative to improve vaccine efficacy. In fact, IRM vaccination studies testing several immune-checkpoint- and agonist-specific antibodies revealed both anti-PD-1 and anti-4-1BB to be beneficial even when a lower IRM dose was combined with cytokines or pharmacological treatments.[11] To further enhance the versatility of the IRM vaccine, we also investigated the importance of inhibiting the binding of the CD47 "don't eat

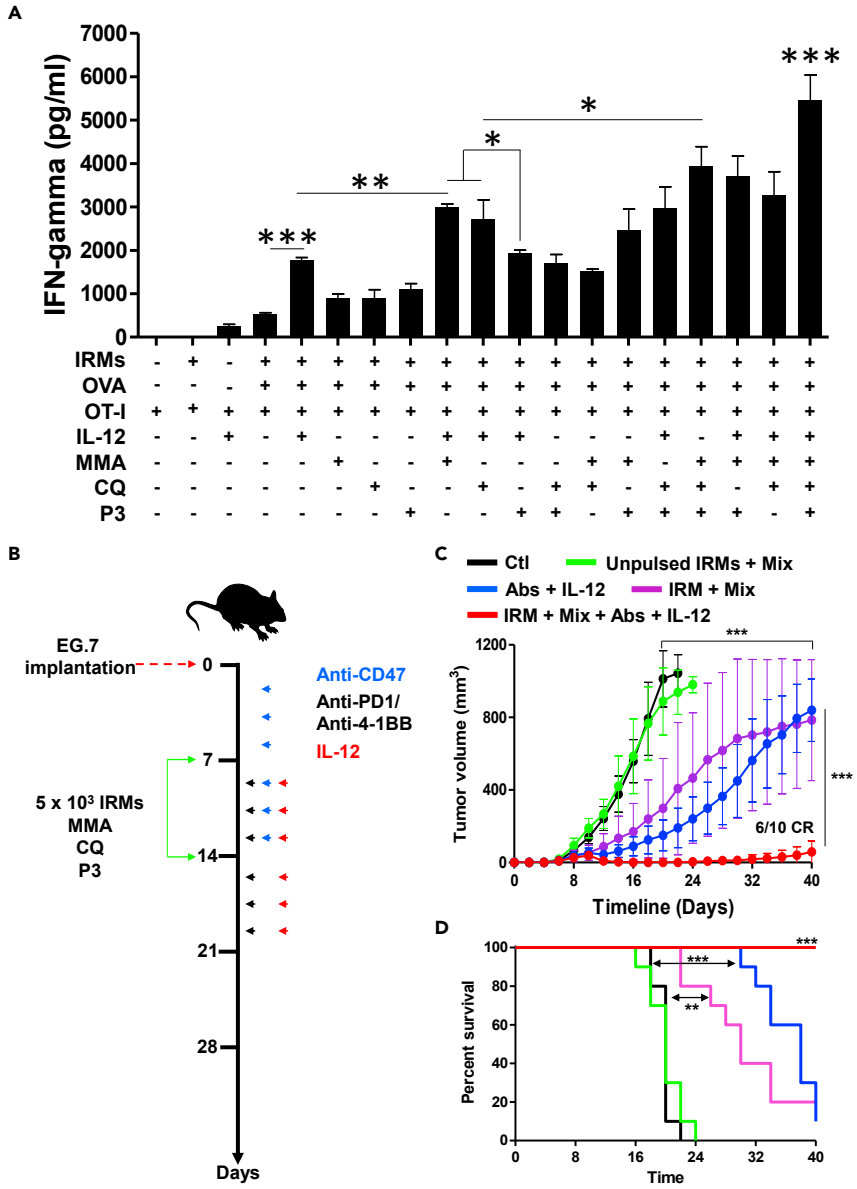

Figure 6. Pharmacologically enhanced IRMs combined with IL-12 and all tested antibodies eradicate established tumors

(A) IFN-gamma quantification from an antigen presentation assay testing treatment with IL-12, MMA, CQ, and p3 as a single treatment with IRMs or in combination.

(B) Schematic diagram showing the study design for the final therapeutic vaccination.

(C) Tumor growth curve of animals vaccinated using 5 × 10^3 pharmacologically enhanced (Mix: CQ, MMA and p3) OVA-pulsed IRMs (purple) versus 5 × 10^3 IRMs pharmacologically enhanced OVA-pulsed IRMs combined with IL-12 and all Abs (red). Non-vaccinated animals receiving the EG.7 tumor cells are shown in black, pharmacologically enhanced (Mix) IRMs (no OVA) in green, and all Abs combined with IL-12 in blue.

(D) The Kaplan-Meier survival curve of the experiment shown in panel (G). For panels C and D, n = 10/group. Results are represented as means with S.D. error bars, and statistical significance is represented with asterisks: *P<0.05, **P<0.01, ***P<0.001.

me" signal to the SIRPα receptor on macrophages as a means to amplify the immune attack on cancer cells, as anti-CD47 monotherapy was previously shown to be beneficial against leukemia, glioblastoma, cervical and ovarian cancer.[35–41] Altogether, investigating additional therapeutic antibodies in development can potentially unveil combos with unheralded synergistic effects.

Limitations of the study

The future of cancer vaccination relies on the design of novel combination strategies. The *CIt* protocol may represent a starting point as it sums up and brings forward a "three-step" approach. Our study is however limited by three main factors. First, our antigen presentation assay identified a series of pro-inflammatory cytokines (IL-2, IL-7, and IL-15) capable of boosting T-cell activation *in vitro*. However, their real potency could only be assessed using *in vivo* models. Likewise, we cannot preclude a powerful anti-tumoral effect if IL-1 or TNF-alpha are co-administered *in vivo* despite inapparent *in vitro* activity. Second, our cellular vaccine requires the use of three therapeutic antibodies. So far, only anti-PD1 (Pembrolizumab or Nivolumab), anti-PD-L1 (Atezolizumab or Avelumab), and anti-CTLA4 (Ipilimumab) are clinically approved. Thus, the *CIt* protocol may be adapted to the future design of vaccines upon approval of the anti-CD47, anti-41BB, and potentially other antibodies currently in development. Finally, all *in vivo* studies were conducted using a single tumor model (EG.7 lymphoma). Therefore, it will be important to conduct follow-up studies using several different tumor models to demonstrate larger applicability of this vaccination protocol.

STAR★METHODS

Detailed methods are provided in the online version of this paper and include the following:

- KEY RESOURCES TABLE
- RESOURCE AVAILABILITY
  - Lead contact
  - Materials availability
  - Data and code availability
- EXPERIMENTAL MODEL AND SUBJECT DETAILS
  - Mice strains
  - Cell lines
  - IRM engineering
  - Routing and dosing studies
  - Vaccination studies
- METHOD DETAILS
  - MTD identification
  - Antigen cross-presentation assay
  - Evaluating antigen uptake and processing by IRMs
  - Assessment of endosomal damages in response to cationic peptide treatments
  - RNA extraction and sequencing
  - Bioinformatics analysis
  - Statistical analysis

SUPPLEMENTAL INFORMATION

Supplemental information can be found online at https://doi.org/10.1016/j.isci.2022.105537.

ACKNOWLEDGMENTS

This work was supported by an operating grant from the Cancer Research Society (#OG834469), an innovation to impact grant from the Canadian Cancer Society (#706201), and a Discovery grant from the National Research and Engineering Council of Canada (#RGPIN/06101-2014). We wish to thank all the personnel from the IRIC animal facility for providing technical help with some of the *in vivo* experiments.

AUTHOR CONTRIBUTIONS

JPB, NEH, and JA conducted most of the *in vitro* and *in vivo* assays. ST, NE, and RS participated in the study design. MR conceived and supervised the project, analyzed data, and wrote the first draft of the article. All authors contributed to the editing of the article.

DECLARATION OF INTERESTS

Competing interests: The authors declare that they have no competing financial interests. A provisional patent has been filed to protect the MSC-IPr (IRM) technology and its applications (#62/835,678).

Received: July 14, 2022
Revised: September 4, 2022
Accepted: November 7, 2022
Published: December 22, 2022

REFERENCES

1. Chakraborty, C., Sharma, A.R., Bhattacharya, M., and Lee, S.S. (2021). From COVID-19 to cancer mRNA vaccines: moving from bench to clinic in the vaccine landscape. Front. Immunol. *12*, 679344. https://doi.org/10.3389/fimmu.2021.679344.

2. Schiller, J.T., Lowy, D.R., Frazer, I.H., Finn, O.J., Vilar, E., Lyerly, H.K., Gnjatic, S., Zaidi, N., Ott, P.A., Balachandran, V.P., et al. (2022). Cancer vaccines. Cancer Cell *40*, 559–564. https://doi.org/10.1016/j.ccell.2022.05.015.

3. Lang, F., Schrörs, B., Löwer, M., Türeci, Ö., and Sahin, U. (2022). Identification of neoantigens for individualized therapeutic cancer vaccines. Nat. Rev. Drug Discov. *21*, 261–282. https://doi.org/10.1038/s41573-021-00387-y.

4. Zheng, Y., Fu, Y., Wang, P.P., and Ding, Z.Y. (2022). Neoantigen: a promising target for the immunotherapy of colorectal cancer. Dis. Markers *2022*, 8270305. https://doi.org/10.1155/2022/8270305.

5. Sharpnack, M.F., Johnson, T.S., Chalkley, R., Han, Z., Carbone, D., Huang, K., and He, K. (2022). TSAFinder: exhaustive tumor-specific antigen detection with RNAseq. Bioinformatics *38*, 2422–2427. https://doi.org/10.1093/bioinformatics/btac116.

6. Shang, S., Zhao, Y., Qian, K., Qin, Y., Zhang, X., Li, T., Shan, L., Wei, M., Xi, J., and Tang, B. (2022). The role of neoantigens in tumor immunotherapy. Biomed. Pharmacother. *151*, 113118. https://doi.org/10.1016/j.biopha.2022.113118.

7. Chai, S., Smith, C.C., Kochar, T.K., Hunsucker, S.A., Beck, W., Olsen, K.S., Vensko, S., Glish, G.L., Armistead, P.M., Prins, J.F., and Vincent, B.G. (2022). NeoSplice: a bioinformatics method for prediction of splice variant neoantigens. Bioinform. Adv. *2*, vbac032. https://doi.org/10.1093/bioadv/vbac032.

8. Shinde, P., Fernandes, S., Melinkeri, S., Kale, V., and Limaye, L. (2018). Compromised functionality of monocyte-derived dendritic cells in multiple myeloma patients may limit their use in cancer immunotherapy. Sci. Rep. *8*, 5705. https://doi.org/10.1038/s41598-018-23943-w.

9. Silk, K.M., Silk, J.D., Ichiryu, N., Davies, T.J., Nolan, K.F., Leishman, A.J., Carpenter, L., Watt, S.M., Cerundolo, V., and Fairchild, P.J. (2012). Cross-presentation of tumour antigens by human induced pluripotent stem cell-derived CD141(+)XCR1+ dendritic cells. Gene Ther. *19*, 1035–1040. https://doi.org/10.1038/gt.2011.177.

10. Sachamitr, P., Hackett, S., and Fairchild, P.J. (2014). Induced pluripotent stem cells: challenges and opportunities for cancer immunotherapy. Front. Immunol. *5*, 176. https://doi.org/10.3389/fimmu.2014.00176.

11. Abusarah, J., Khodayarian, F., El-Hachem, N., Salame, N., Olivier, M., Balood, M., Roversi, K., Talbot, S., Bikorimana, J.P., Chen, J., et al. (2021). Engineering immunoproteasome-expressing mesenchymal stromal cells: a potent cellular vaccine for lymphoma and melanoma in mice. Cell Rep. Med. *2*, 100455. https://doi.org/10.1016/j.xcrm.2021.100455.

12. Sun, X., Zeng, L., and Huang, Y. (2019). Transcutaneous delivery of DNA/mRNA for cancer therapeutic vaccination. J. Gene Med. *21*, e3089. https://doi.org/10.1002/jgm.3089.

13. Shemesh, C.S., Hsu, J.C., Hosseini, I., Shen, B.Q., Rotte, A., Twomey, P., Girish, S., and Wu, B. (2021). Personalized cancer vaccines: clinical landscape, challenges, and opportunities. Mol. Ther. *29*, 555–570. https://doi.org/10.1016/j.ymthe.2020.09.038.

14. Ding, Y., Li, Z., Jaklenec, A., and Hu, Q. (2021). Vaccine delivery systems toward lymph nodes. Adv. Drug Deliv. Rev. *179*, 113914. https://doi.org/10.1016/j.addr.2021.113914.

15. Bolhassani, A., Safaiyan, S., and Rafati, S. (2011). Improvement of different vaccine delivery systems for cancer therapy. Mol. Cancer *10*, 3. https://doi.org/10.1186/1476-4598-10-3.

16. Haring, J.S., Badovinac, V.P., and Harty, J.T. (2006). Inflaming the CD8+ T cell response. Immunity *25*, 19–29. https://doi.org/10.1016/j.immuni.2006.07.001.

17. Cox, M.A., and Zajac, A.J. (2010). Shaping successful and unsuccessful CD8 T cell responses following infection. J. Biomed. Biotechnol. *2010*, 159152. https://doi.org/10.1155/2010/159152.

18. Mardani, F., Saad, W., El-Hachem, N., Bikorimana, J.P., Kurdi, M., Shammaa, R., Talbot, S., and Rafei, M. (2022). LSD1 inhibition enhances the immunogenicity of mesenchymal stromal cells by eliciting a dsRNA stress response. Cells *11*, 1816. https://doi.org/10.3390/cells11111816.

19. Salame, N., Bikorimana, J.P., El-Hachem, N., Saad, W., Kurdi, M., Zhao, J., Eliopoulos, N., Shammaa, R., and Rafei, M. (2022). UM171A-induced ROS promote antigen cross-presentation of immunogenic peptides by bone marrow-derived mesenchymal stromal cells. Stem Cell Res. Ther. *13*, 16. https://doi.org/10.1186/s13287-021-02693-z.

20. Koenis, D.S., Medzikovic, L., van Loenen, P.B., van Weeghel, M., Huveneers, S., Vos, M., Evers-van Gogh, I.J., Van den Bossche, J., Speijer, D., Kim, Y., et al. (2018). Nuclear receptor Nur77 limits the macrophage inflammatory response through transcriptional reprogramming of mitochondrial metabolism. Cell Rep. *24*, 2127–2140.e7. https://doi.org/10.1016/j.celrep.2018.07.065.

21. Jha, A.K., Huang, S.C.C., Sergushichev, A., Lampropoulou, V., Ivanova, Y., Loginicheva, E., Chmielewski, K., Stewart, K.M., Ashall, J., Everts, B., et al. (2015). Network integration of parallel metabolic and transcriptional data reveals metabolic modules that regulate macrophage polarization. Immunity *42*, 419–430. https://doi.org/10.1016/j.immuni.2015.02.005.

22. Mills, E.L., Kelly, B., Logan, A., Costa, A.S.H., Varma, M., Bryant, C.E., Tourlomousis, P., Däbritz, J.H.M., Gottlieb, E., Latorre, I., et al. (2016). Succinate dehydrogenase supports metabolic repurposing of mitochondria to drive inflammatory macrophages. Cell *167*, 457–470.e13. https://doi.org/10.1016/j.cell.2016.08.064.

23. Ryan, D.G., and O'Neill, L.A.J. (2017). Krebs cycle rewired for macrophage and dendritic cell effector functions. FEBS Lett. *591*, 2992–3006. https://doi.org/10.1002/1873-3468.12744.

24. El-Kadiry, A.E.H., Beaudoin, S., Plouffe, S., and Rafei, M. (2022). Accum™ technology: a novel conjugable primer for onco-immunotherapy. Molecules *27*, 3807. https://doi.org/10.3390/molecules27123807.

25. Bikorimana, J.P., Salame, N., Beaudoin, S., Balood, M., Crosson, T., Abusarah, J., Talbot, S., Löbenberg, R., Plouffe, S., and Rafei, M. (2022). Promoting antigen escape from dendritic cell endosomes potentiates anti-tumoral immunity. Cell Rep. Med. *3*, 100534. https://doi.org/10.1016/j.xcrm.2022.100534.

26. Akishiba, M., Takeuchi, T., Kawaguchi, Y., Sakamoto, K., Yu, H.H., Nakase, I., Takatani-Nakase, T., Madani, F., Gräslund, A., and Futaki, S. (2017). Cytosolic antibody delivery by lipid-sensitive endosomolytic peptide. Nat. Chem. *9*, 751–761. https://doi.org/10.1038/nchem.2779.

27. Dingjan, I., Verboogen, D.R., Paardekooper, L.M., Revelo, N.H., Sittig, S.P., Visser, L.J., Mollard, G.F.v., Henriet, S.S., Figdor, C.G., Ter Beest, M., and van den Bogaart, G. (2016). Lipid peroxidation causes endosomal antigen release for cross-presentation. Sci. Rep. *6*, 22064. https://doi.org/10.1038/srep22064.

28. Shammaa, R., El-Kadiry, A.E.H., Abusarah, J., and Rafei, M. (2020). Mesenchymal stem cells beyond regenerative medicine. Front. Cell Dev. Biol. *8*, 72. https://doi.org/10.3389/fcell.2020.00072.

29. Rafei, M., Hsieh, J., Fortier, S., Li, M., Yuan, S., Birman, E., Forner, K., Boivin, M.N., Doody,

K., Tremblay, M., et al. (2008). Mesenchymal stromal cell-derived CCL2 suppresses plasma cell immunoglobulin production via STAT3 inactivation and PAX5 induction. Blood *112*, 4991–4998. https://doi.org/10.1182/blood-2008-07-166892.

30. Rafei, M., Birman, E., Forner, K., and Galipeau, J. (2009). Allogeneic mesenchymal stem cells for treatment of experimental autoimmune encephalomyelitis. Mol. Ther. *17*, 1799–1803. https://doi.org/10.1038/mt.2009.157.

31. El-Kadiry, A.E.H., Rafei, M., and Shammaa, R. (2021). Cell therapy: types, regulation, and clinical benefits. Front. Med. *8*, 756029. https://doi.org/10.3389/fmed.2021.756029.

32. Pang, S.H.M., D'Rozario, J., Mendonca, S., Bhuvan, T., Payne, N.L., Zheng, D., Hisana, A., Wallis, G., Barugahare, A., Powell, D., et al. (2021). Mesenchymal stromal cell apoptosis is required for their therapeutic function. Nat. Commun. *12*, 6495. https://doi.org/10.1038/s41467-021-26834-3.

33. Galleu, A., Riffo-Vasquez, Y., Trento, C., Lomas, C., Dolcetti, L., Cheung, T.S., von Bonin, M., Barbieri, L., Halai, K., Ward, S., et al. (2017). Apoptosis in mesenchymal stromal cells induces *in vivo* recipient-mediated immunomodulation. Sci. Transl. Med. *9*, eaam7828. https://doi.org/10.1126/scitranslmed.aam7828.

34. Bikorimana, J.P., Abusarah, J., Salame, N., El-Hachem, N., Shammaa, R., and Rafei, M. (2022). Humoral immunity to allogeneic immunoproteasome-expressing mesenchymal stromal cells requires efferocytosis by endogenous phagocytes. Cells *11*, 596. https://doi.org/10.3390/cells11040596.

35. Veillette, A., and Chen, J. (2018). SIRPα-CD47 immune checkpoint blockade in anticancer therapy. Trends Immunol. *39*, 173–184. https://doi.org/10.1016/j.it.2017.12.005.

36. Upton, R., Banuelos, A., Feng, D., Biswas, T., Kao, K., McKenna, K., Willingham, S., Ho, P.Y., Rosental, B., Tal, M.C., et al. (2021). Combining CD47 blockade with trastuzumab eliminates HER2-positive breast cancer cells and overcomes trastuzumab tolerance. Proc. Natl. Acad. Sci. USA *118*. e2026849118. https://doi.org/10.1073/pnas.2026849118.

37. Murata, Y., Saito, Y., Kotani, T., and Matozaki, T. (2018). CD47-signal regulatory protein α signaling system and its application to cancer immunotherapy. Cancer Sci. *109*, 2349–2357. https://doi.org/10.1111/cas.13663.

38. Logtenberg, M.E.W., Scheeren, F.A., and Schumacher, T.N. (2020). The CD47-SIRPα immune checkpoint. Immunity *52*, 742–752. https://doi.org/10.1016/j.immuni.2020.04.011.

39. Gauttier, V., Pengam, S., Durand, J., Biteau, K., Mary, C., Morello, A., Néel, M., Porto, G., Teppaz, G., Thepenier, V., et al. (2020). Selective SIRPα blockade reverses tumor T cell exclusion and overcomes cancer immunotherapy resistance. J. Clin. Invest. *130*, 6109–6123. https://doi.org/10.1172/jci135528.

40. Feng, M., Jiang, W., Kim, B.Y.S., Zhang, C.C., Fu, Y.X., and Weissman, I.L. (2019). Phagocytosis checkpoints as new targets for cancer immunotherapy. Nat. Rev. Cancer *19*, 568–586. https://doi.org/10.1038/s41568-019-0183-z.

41. Candas-Green, D., Xie, B., Huang, J., Fan, M., Wang, A., Menaa, C., Zhang, Y., Zhang, L., Jing, D., Azghadi, S., et al. (2020). Dual blockade of CD47 and HER2 eliminates radioresistant breast cancer cells. Nat. Commun. *11*, 4591. https://doi.org/10.1038/s41467-020-18245-7.

42. Yu, J., Sun, H., Cao, W., Song, Y., and Jiang, Z. (2022). Research progress on dendritic cell vaccines in cancer immunotherapy. Exp. Hematol. Oncol. *11*, 3. https://doi.org/10.1186/s40164-022-00257-2.

43. Wylie, B., Ong, F., Belhoul-Fakir, H., Priebatsch, K., Bogdawa, H., Stirnweiss, A., Watt, P., Cunningham, P., Stone, S.R., and Waithman, J. (2021). Targeting cross-presentation as a route to improve the efficiency of peptide-based cancer vaccines. Cancers *13*, 6189. https://doi.org/10.3390/cancers13246189.

44. Tang, L., Zhang, R., Zhang, X., and Yang, L. (2021). Personalized neoantigen-pulsed DC vaccines: advances in clinical applications. Front. Oncol. *11*, 701777. https://doi.org/10.3389/fonc.2021.701777.

45. Plumas, J. (2022). Harnessing dendritic cells for innovative therapeutic cancer vaccines. Curr. Opin. Oncol. *34*, 161–168. https://doi.org/10.1097/cco.0000000000000815.

46. Johnson, P., Rosendahl, N., and Radford, K.J. (2022). Conventional type 1 dendritic cells (cDC1) as cancer therapeutics: challenges and opportunities. Expert Opin. Biol. Ther. *22*, 465–472. https://doi.org/10.1080/14712598.2022.1994943.

47. Filin, I.Y., Kitaeva, K.V., Rutland, C.S., Rizvanov, A.A., and Solovyeva, V.V. (2021). Recent advances in experimental dendritic cell vaccines for cancer. Front. Oncol. *11*, 730824. https://doi.org/10.3389/fonc.2021.730824.

48. Dzau, V.J., Balatbat, C.A., and Offodile, A.C., 2nd (2022). Closing the global vaccine equity gap: equitably distributed manufacturing. Lancet *399*, 1924–1926. https://doi.org/10.1016/s0140-6736(22)00793-0.

49. Yu, T.W., Chueh, H.Y., Tsai, C.C., Lin, C.T., and Qiu, J.T. (2016). Novel GM-CSF-based vaccines: one small step in GM-CSF gene optimization, one giant leap for human vaccines. Hum. Vaccin. Immunother. *12*, 3020–3028. https://doi.org/10.1080/21645515.2016.1221551.

50. Xia, D., Li, F., and Xiang, J. (2004). Engineered fusion hybrid vaccine of IL-18 gene-modified tumor cells and dendritic cells induces enhanced antitumor immunity. Cancer Biother. Radiopharm. *19*, 322–330. https://doi.org/10.1089/1084978041424990.

51. Tang, Z.H., Qiu, W.H., Wu, G.S., Yang, X.P., Zou, S.Q., and Qiu, F.Z. (2002). The immunotherapeutic effect of dendritic cells vaccine modified with interleukin-18 gene and tumor cell lysate on mice with pancreatic carcinoma. World J. Gastroenterol. *8*, 908–912. https://doi.org/10.3748/wjg.v8.i5.908.

52. Baek, S., Kim, Y.M., Kim, S.B., Kim, C.S., Kwon, S.W., Kim, Y., Kim, H., and Lee, H. (2015). Therapeutic DC vaccination with IL-2 as a consolidation therapy for ovarian cancer patients: a phase I/II trial. Cell. Mol. Immunol. *12*, 87–95. https://doi.org/10.1038/cmi.2014.40.

53. Kirkling, M.E., Cytlak, U., Lau, C.M., Lewis, K.L., Resteu, A., Khodadadi-Jamayran, A., Siebel, C.W., Salmon, H., Merad, M., Tsirigos, A., et al. (2018). Notch signaling facilitates *in vitro* generation of cross-presenting classical dendritic cells. Cell Rep. *23*, 3658–3672.e6. https://doi.org/10.1016/j.celrep.2018.05.068.

54. Nizzoli, G., Krietsch, J., Weick, A., Steinfelder, S., Facciotti, F., Gruarin, P., Bianco, A., Steckel, B., Moro, M., Crosti, M., et al. (2013). Human CD1c+ dendritic cells secrete high levels of IL-12 and potently prime cytotoxic T-cell responses. Blood *122*, 932–942. https://doi.org/10.1182/blood-2013-04-495424.

55. Melchionda, F., Fry, T.J., Milliron, M.J., McKirdy, M.A., Tagaya, Y., and Mackall, C.L. (2005). Adjuvant IL-7 or IL-15 overcomes immunodominance and improves survival of the CD8+ memory cell pool. J. Clin. Invest. *115*, 1177–1187. https://doi.org/10.1172/jci23134.

56. Levin, A.M., Bates, D.L., Ring, A.M., Krieg, C., Lin, J.T., Su, L., Moraga, I., Raeber, M.E., Bowman, G.R., Novick, P., et al. (2012). Exploiting a natural conformational switch to engineer an interleukin-2 'superkine'. Nature *484*, 529–533. https://doi.org/10.1038/nature10975.

57. Silva, D.A., Yu, S., Ulge, U.Y., Spangler, J.B., Jude, K.M., Labão-Almeida, C., Ali, L.R., Quijano-Rubio, A., Ruterbusch, M., Leung, I., et al. (2019). De novo design of potent and selective mimics of IL-2 and IL-15. Nature *565*, 186–191. https://doi.org/10.1038/s41586-018-0830-7.

58. Sharma, M., Khong, H., Fa'ak, F., Bentebibel, S.E., Janssen, L.M.E., Chesson, B.C., Creasy, C.A., Forget, M.A., Kahn, L.M.S., Pazdrak, B., et al. (2020). Bempegaldesleukin selectively depletes intratumoral Tregs and potentiates T cell-mediated cancer therapy. Nat. Commun. *11*, 661. https://doi.org/10.1038/s41467-020-14471-1.

59. Ptacin, J.L., Caffaro, C.E., Ma, L., San Jose Gall, K.M., Aerni, H.R., Acuff, N.V., Herman, R.W., Pavlova, Y., Pena, M.J., Chen, D.B., et al. (2021). An engineered IL-2 reprogrammed for anti-tumor therapy using a semi-synthetic organism. Nat. Commun. *12*, 4785. https://doi.org/10.1038/s41467-021-24987-9.

60. Doberstein, S.K. (2019). Bempegaldesleukin (NKTR-214): a CD-122-biased IL-2 receptor agonist for cancer immunotherapy. Expert Opin. Biol. Ther. *19*, 1223–1228. https://doi.org/10.1080/14712598.2019.1685489.

61. Charych, D.H., Hoch, U., Langowski, J.L., Lee, S.R., Addepalli, M.K., Kirk, P.B., Sheng, D., Liu, X., Sims, P.W., VanderVeen, L.A., et al. (2016). NKTR-214, an engineered cytokine with biased IL2 receptor binding, increased tumor exposure, and marked efficacy in mouse tumor models. Clin. Cancer Res. *22*, 680–690. https://doi.org/10.1158/1078-0432.Ccr-15-1631.

62. Williams, P., Rafei, M., Bouchentouf, M., Raven, J., Yuan, S., Cuerquis, J., Forner, K.A., Birman, E., and Galipeau, J. (2010). A fusion of GMCSF and IL-21 initiates hypersignaling through the IL-21Ralpha chain with immune activating and tumoricidal effects *in vivo*. Mol. Ther. *18*, 1293–1301. https://doi.org/10.1038/mt.2010.49.

63. Williams, P., Bouchentouf, M., Rafei, M., Romieu-Mourez, R., Hsieh, J., Boivin, M.N., Yuan, S., Forner, K.A., Birman, E., and Galipeau, J. (2010). A dendritic cell population generated by a fusion of GM-CSF and IL-21 induces tumor-antigen-specific immunity. J. Immunol. *185*, 7358–7366. https://doi.org/10.4049/jimmunol.1002201.

64. Rafei, M., Rouette, A., Brochu, S., Vanegas, J.R., and Perreault, C. (2013). Differential effects of γc cytokines on postselection differentiation of CD8 thymocytes. Blood *121*, 107–117. https://doi.org/10.1182/blood-2012-05-433508.

65. Rafei, M., and Galipeau, J. (2010). A CCL2-based fusokine as a novel biopharmaceutical for the treatment of CCR2-driven autoimmune diseases. Crit. Rev. Immunol. *30*, 449–461. https://doi.org/10.1615/critrevimmunol.v30.i5.40.

66. Embgenbroich, M., and Burgdorf, S. (2018). Current concepts of antigen cross-presentation. Front. Immunol. *9*, 1643. https://doi.org/10.3389/fimmu.2018.01643.

67. Alloatti, A., Rookhuizen, D.C., Joannas, L., Carpier, J.M., Iborra, S., Magalhaes, J.G., Yatim, N., Kozik, P., Sancho, D., Albert, M.L., and Amigorena, S. (2017). Critical role for Sec22b-dependent antigen cross-presentation in antitumor immunity. J. Exp. Med. *214*, 2231–2241. https://doi.org/10.1084/jem.20170229.

68. Han, D., Liu, J., Chen, C., Dong, L., Liu, Y., Chang, R., Huang, X., Liu, Y., Wang, J., Dougherty, U., et al. (2019). Anti-tumour immunity controlled through mRNA m(6)A methylation and YTHDF1 in dendritic cells. Nature *566*, 270–274. https://doi.org/10.1038/s41586-019-0916-x.

69. Fouda, A., Tahsini, M., Khodayarian, F., Al-Nafisah, F., and Rafei, M. (2017). A fluorescence-based lymphocyte assay suitable for high-throughput screening of small molecules. J Vis Exp, 55199. https://doi.org/10.3791/55199.

70. Belabed, M., Mauvais, F.X., Maschalidi, S., Kurowska, M., Goudin, N., Huang, J.D., Fischer, A., de Saint Basile, G., van Endert, P., Sepulveda, F.E., and Ménasché, G. (2020). Kinesin-1 regulates antigen cross-presentation through the scission of tubulations from early endosomes in dendritic cells. Nat. Commun. *11*, 1817. https://doi.org/10.1038/s41467-020-15692-0.

71. Hobo, W., Maas, F., Adisty, N., de Witte, T., Schaap, N., van der Voort, R., and Dolstra, H. (2010). siRNA silencing of PD-L1 and PD-L2 on dendritic cells augments expansion and function of minor histocompatibility antigen-specific CD8+ T cells. Blood *116*, 4501–4511. https://doi.org/10.1182/blood-2010-04-278739.

72. Yu, G., Wang, L.G., Han, Y., and He, Q.Y. (2012). clusterProfiler: an R package for comparing biological themes among gene clusters. OMICS *16*, 284–287. https://doi.org/10.1089/omi.2011.0118.

73. Ritchie, M.E., Phipson, B., Wu, D., Hu, Y., Law, C.W., Shi, W., and Smyth, G.K. (2015). Limma powers differential expression analyses for RNA-sequencing and microarray studies. Nucleic Acids Res. *43*, e47. https://doi.org/10.1093/nar/gkv007.

74. Subramanian, A., Tamayo, P., Mootha, V.K., Mukherjee, S., Ebert, B.L., Gillette, M.A., Paulovich, A., Pomeroy, S.L., Golub, T.R., Lander, E.S., and Mesirov, J.P. (2005). Gene set enrichment analysis: a knowledge-based approach for interpreting genome-wide expression profiles. Proc. Natl. Acad. Sci. USA. *102*, 15545–15550. https://doi.org/10.1073/pnas.0506580102.

75. Wu, T., Hu, E., Xu, S., Chen, M., Guo, P., Dai, Z., Feng, T., Zhou, L., Tang, W., Zhan, L., et al. (2021). clusterProfiler 4.0: a universal enrichment tool for interpreting omics data. Innovation *2*, 100141. https://doi.org/10.1016/j.xinn.2021.100141.

STAR★METHODS

KEY RESOURCES TABLE

REAGENT or RESOURCE	SOURCE	IDENTIFIER
Antibodies		
BV421 Mouse Anti-Mouse H-2K[b]	BD Biosciences	Cat#: 562942, RRID:AB_2737908
Anti-CD47	Bio X cell	Cat#: BE0270, RRID:AB_2687793
InVivoMAb anti-mouse PD-1 (CD279)	Bio X cell	Cat#: BE0146, RRID:AB_10949053
InVivoPlus anti-mouse 4-1BB (CD137)	BioXCell	CAT# BP0239, RRID:AB_2924874
Chemicals, peptides, and recombinant proteins		
Recombinant Murine IL1β	PeproTech	Cat#: 211-11B
Recombinant Murine IL-2	PeproTech	Cat#: 212-12
Recombinant Murine IL-7	PeproTech	Cat#: 217-17
Recombinant Murine IL-12 p70	PeproTech	Cat#: 210-12
Recombinant Murine IL-15	PeproTech	Cat#: 210-15
Recombinant Murine IL-21	PeproTech	Cat#: 210-21
Recombinant Murine IFN-γ	PeproTech	Cat#: 315-05
Recombinant Murine TNF-alpha	PeproTech	Cat#: 315-01A
Albumin from chicken egg white	Sigma-Aldrich	Cat#: A5503
Accutase® solution	Sigma-Aldrich	Cat#: A6964
Cytochrome c from equine heart	Sigma-Aldrich	Cat#: C2506
Chloroquine diphosphate salt	Sigma-Aldrich	Cat#: C6628
Methylmalonic acid	Sigma-Aldrich	Cat#: M54058
CCF4-AM	ThermoFisher Scientific	Cat#: K1029
DQ™ ovalbumin	ThermoFisher Scientific	Cat#: D12053
Ovalbumin, Alexa Fluor™ 647 Conjugate	ThermoFisher Scientific	Cat#: O34784
Bovine Serum Albumin (BSA)	Bio Basic Canada Inc.	CAS#: 9048-46-8
β-Mercaptoethanol	Gibco	Cat#: 21985023
Sodium Pyruvate	Multicell	Cat#: 600-110-EL
Fetal Bovin Serum (FBS)	Multicell	Cat#: 090150
Phosphate Buffered Saline (PBS)	Multicell	Cat#: 311-010-CL
RPMI 1640	Multicell	Cat#: 350-000-CL
Penicillin/ Streptomycin	Multicell	Cat#: 450-201-EL
L-glutamine	Multicell	Cat#: 609-065-EL
HEPES	Multicell	Cat#: 330-050-EL
MEM essential amino acid	Multicell	Cat#: 321-011-EL
DMEM	Multicell	Cat#: 319-005-CL
Critical commercial assays		
RNeasy Mini Kit[50]	Qiagen	Cat#:74104
Mouse IFN-gamma Quantikine ELISA Kit	R&D systems	Cat#: MIF00
EasySep™ Mouse CD8a Positive Selection Kit II	Stemcell Technologies	Cat#:18753
APC Annexin V Apoptosis Detection Kit with PI	BioLegend	Cat#: 640932
Deposited data		
RNA-seq data (MSCs, IRMs)	GEO	GSE183055
RNA-seq Data (DCs)	GEO	GSE158783

(*Continued on next page*)

Continued

REAGENT or RESOURCE	SOURCE	IDENTIFIER
Experimental models: Cell lines		
Mouse: E.G7-OVA [derivative of EL4]	ATCC	ATCC Cat# CRL-2113, RRID: CVCL_3505
Experimental models: Organisms/strains		
Mouse: C57BL/6NCrl	The Jackson Laboratory	Strain #000664
Mouse: OT-I (C57BL/6-Tg (TcraTcrb)1100Mjb/J)	The Jackson Laboratory	Strain #003831
Recombinant DNA		
IWLTALKFLGKHAAKHLAKQQLSKL-C	Genscript	N/A
IWLTALKFLGKHAAKHDAKQQLSKL-C	Experimental models: Cell lines	N/A
IWLTALKFLGKHAAKHEAKQQLSKL-C	Genscript	N/A
Software and algorithms		
FlowJo v10	FlowJo™	https://www.flowjo.com/solutions/flowjo/downloads
Prism-GraphPad	GraphPad Software	https://www.graphpad.com/scientific-software/prism/
Bioinformatics software(s)	R statistical programming Other packages Pheatmap Ggplot2 ClusterProfiler	https://www.r-project.org/https://cran.r-project.org/web/packages/pheatmap/index.html https://cran.r-project.org/web/packages/ggplot2/index.html https://bioconductor.org/packages/release/bioc/html/clusterProfiler.html

RESOURCE AVAILABILITY

Lead contact

Further information and requests for resources and reagents should be directed to and will be fulfilled by the Lead Contact, Moutih Rafei (moutih.rafei.1@umontreal.ca).

Materials availability

The IRM cells used in this study will be made available on request, but we may require a payment and/or a completed Material Transfer Agreement if there is potential for commercial application.

Data and code availability

- RNA-seq data have been deposited at GEO and are publicly available as of the date of publication. Accession numbers are listed in the key resources table. Database: GSE183055, GSE158783.
- Any additional information required to reanalyze the data reported in this paper is available from the lead contact upon request.
- This paper does not report original code. Any analyses applied are based on previously available software and established R packages, primarily, custom R scripts: https://www.R-project.org/, ggplot2 and cluster profiler.[72]

EXPERIMENTAL MODEL AND SUBJECT DETAILS

Mice strains

For all experiments, six- to ten-week-old female C57BL/6 and OT-1 (B6.129P2-H2-K1^{tm1Bpe} H2-D1^{tm1Bpe}/DcrJ) were purchased from The Jackson Laboratory (Bar Harbor, ME, USA). The mice were housed and maintained in accordance with the guidelines approved by the Animal Care Committee of Université de Montréal in a pathogen-free environment at the animal facility of the Institute for Research in Immunology

and Cancer (IRIC). Animal protocols were approved by the Animal Care Committee of Université de Montréal.

Cell lines

Tumor cells EG.7 used in this study were a kind gift from Dr. Jacques Galipeau (University of Wisconsin-Madison, WI, USA). E.G7 cells were cultured RPMI 1460 supplemented with 2 g/L Glucose, 10% FBS, 50 U/mL Penicillin-Streptomycin, 2 mM L-glutamine, 10mM HEPES, 1mM Sodium Pyruvate, and 0.5 mM β-Mercaptoethanol, and kept under selection using 80 mg/mL of G418.

IRM engineering

IRM cells were previously generated by engineering bone marrow derived MSCs in the lab of Dr. Moutih Rafei as detailed by Abusarah et al.[11] Briefly, bone marrow derived primary MSCs were isolated from the femur of a female C57BL/6 mouse, expanded and evaluated for the expression of CD44, CD45, CD73, CD90 and CD105 and for their osteogenic and adipogenic differentiation. To engineer the MSCs, a construct containing the three inducible subunits of the murine immunoproteasome (β1i, β2i, and β5i) separated by the viral T2A sequence was generated and co-transfected along with the VSV-G vector encoding the envelop protein into the retroviral packaging cell line GP2-293 using PolyFect® according to the manufacturer's protocol. A concentrated dose of the retrovirus was produced by ultracentrifugation of the cell supernatant containing the virus which was collected at 48- and 72-h post-transfection. Early passage MSCs were plated at 50–60% confluency in a 12 well plate and transduced overnight using media containing the concentrated virus. The initial transduction was followed by two more transductions after the recovery and proliferation of the cells. Upon verifying successful transduction and expression of the three subunits of the immunoproteasome via immunoblotting, the cells were re-evaluated for the expression of CD44, CD45, CD73, CD90 and CD105 and for their osteogenic and adipogenic differentiation.[11] Successfully transduced MSCs, now referred to as IRMs, were sorted, expanded and frozen in liquid nitrogen. The same steps were followed, but using the construct backbone, to generate the control (Ctrl) MSCs for this study. All cells were maintained at 37°C in a 5% CO_2 incubator. All cell culture media and reagents were purchased from Wisent Bioproducts (St-Bruno, QC, Canada).

Routing and dosing studies

To identify the best dosing and route of administration for all subsequent *in vivo* studies, C57BL/6-derived IRMs were tested at various doses (1.0, 0.5, 0.25, 0.1, 0.05, or 0.005 × 10^6 cells) and delivered to each mouse on days 0 and 14. Cells were injected either via IP or SC route. Two weeks following the second immunization, each mouse received an SC injection containing 5 × 10^5 EG.7 tumor cells. Tumor size and animal survival was followed thereafter until reaching endpoints (ulceration or a tumor volume $\geq$1000 mm^3). Control mice received the challenge with tumor cells only. The mice were monitored for up to 6 weeks. Partial response was defined as mice with delayed or controlled/stabilized tumor growth whereas complete response implied tumor regression following treatment.

Vaccination studies

For animal vaccination, IRMs were pulsed with 5 mg/mL OVA for 9 h. At the end of pulsation time, the cells were washed with PBS, detached using Accutase®, then counted and washed twice with PBS to prepare them for injection. For prophylactic vaccination, each C57BL/6 mouse received 5 × 10^3 cells delivered by SC injection, (n=10/group). The mice in each vaccination group received two doses of the same vaccine on days 0 and 14 (on the same flank). Two weeks following the second dose (day 28), the mice were challenged with 5 × 10^5 E.G7 tumor cells delivered via SC injection (same flank). For all experiments related to the use of IL-12, the cytokine dose was 0.005 mg/kg, administered IP 3 times per week following the first and second injections on days 0 and 14. Control mice received two PBS injections instead of IRMs whereas control mice received tumor cells alone. For therapeutic vaccination, C57BL/6 mice (n=10/group) were first SC-implanted with 2 × 10^5 EG.7 tumor cells. Three days later (or after appearance of palpable tumors with an average size of ~10–30 mm^3), the mice were SC-injected on the same flank with 5 × 10^3 IRMs pulsed with 5 mg/mL OVA for 9h and prepared as mentioned above. Each mouse received two injections separated by 1 week. Control mice received tumor cells alone. For vaccination studies involving MMA, CQ and p3 treatments, IRMs were treated *in vitro* with these agents before or during pulsing for 9h. When the cells were ready to be injected, they were detached using Accutase®, washed, and injected into animals. IL-12 or antibody treatments were then delivered according to provided schedules. Tumor size and animal survival was

followed thereafter using a digital caliber until reaching endpoints (ulceration or a tumor volume ≥ 1000 mm^3). For vaccination studies using CD47-treated IRMs, the cells were first incubated with the anti-CD47 antibody at a dilution of 1:200 for 20 min at 4°C. Following incubation time, the cells were washed twice with PBS prior to SC delivery. For vaccination in combination with the immune-checkpoint inhibitor (anti-PD-1), the antibody agonist (anti-4-1BB) or the efferocytosis-blocking anti-CD47 antibody, all antibodies or their relative isotype were delivered IP at 200 μg/mouse 3 times per week for two consecutive weeks. All vaccinated animals were monitored for up to 6 weeks.

METHOD DETAILS

MTD identification

To identify the MTD for CQ, MMA and TC, 5 × 10^4 plated IRMs were treated with ascending doses of the compounds for 24 h. Treated cells were then washed, detached using Accutase® and counted using Trypan Blue to differentiate between live and dead cells. The highest dose with no cell toxicity or decreased proliferation effects was selected for subsequent studies.

Antigen cross-presentation assay

The antigen cross-presentation assay using the OVA protein was performed according to the protocol published by Abusarah et al.[11] Briefly, 1.5 × 10^4 IRMs were seeded per well in a 24-well plate. Adherent cells were pulsed on the following day with 5 mg/mL of OVA for 9 h followed by media removal, and the addition of 1 ×10^5 CD8 T-cells purified from the spleen of an OT-I mouse using positive selection kit according to the manufacturer's instructions. For experiments testing the effects of CQ, MMA, or TC, the treatments were initiated 12 h prior to OVA pulsing. The drugs were present during OVA pulsing incubation period. For the cationic peptides, 100 μM were mixed directly with the OVA protein prior to IRM pulsing. The supernatants of the co-cultures were collected three days later, then quantified for IFN-gamma production using a Quantikine ELISA kit following manufacturer's instructions. For antigen presentation assay conducted in the presence of cytokines, each corresponding cytokine was added with the OT-I T cells (following OVA pulsing and washing) at the following concentrations: IL-1β (0.01 ng/mL), IL-2 (0.4 ng/mL), IL-7 (0.3 ng/mL), IL-12 (0.1 ng/mL), IL-15 (15 ng/mL), IL-21 (8 ng/mL) and TNF-α (0.05 ng/mL). All used concentrations were previously identified using an antigen presentation assay.

Evaluating antigen uptake and processing by IRMs

OVA uptake and processing was conducted following a previously published protocol.[11,18,19,25] Briefly, 4 × 10^4 IRMs/well were plated in a 12-well plate. On the following day, 1 μg/mL of Alexa Fluor® 647-conjugated OVA was mixed with the selected cationic peptide at 100 μM prior to its addition on IRMs for 9h. At the end of the incubation period, IRMs were detached using Accutase® and washed twice with cold 2% FBS in PBS prior to monitoring their fluorescence using BD FACS Diva on CANTOII. For evaluating the processing of the OVA protein, 10 μg/mL OVA-DQ was mixed with 100 μM of the cationic peptide prior to IRM pulsing. The cells were washed 30 min later, and regular media was added. Two hours later, the treated cells were detached and washed with cold PBS containing 2% FBS prior to fluorescence signal monitoring using BD FACS Diva on CANTOII and analyzed using FlowJoV10.

Assessment of endosomal damages in response to cationic peptide treatments

Endosomal leakage was assessed using two different approaches; the first strategy utilizes the FRET sensor CCF4-AM, a β-lactamase substrate. Briefly, IRMs were treated with 1 μM CCF4-AM for 1 h followed by the addition of 10 mg/mL of β-lactamase in the presence or absence of one of the three cationic peptides (at concentration of 100 μM) for 3 h at 37°C. The cells were then washed, and fresh media added for an incubation period of 16 h at 37°C. The loss of FRET signal between the coumarin (donor) and fluorescein (acceptor) fluorophores was quantified by flow cytometry. For the apoptosis assay, 10^5 IRMs were first supplemented with 10 mg/mL of exogenous rCyt-C for 6 h at 37°C in the presence or absence of the cationic peptide (at the concentration 100 μM). Once the incubation period completed, the cells were collected using Accutase®, washed with ice cold PBS, then stained for Annexin-V according to manufacturer's instructions prior to analysis using BD FACS Diva on CANTOII.

RNA extraction and sequencing

Total RNA was isolated from 10^6 cells for each group using RNeasy® mini kit (QIAGEN) according to manufacturer's instructions. The collected RNA was then evaluated for contamination using nanodrop to read

260/280 and 260/230 ratios, quantified using QuBit (ABI) and the quality assessed with the BioAnalyzer Nano (Agilent) to ensure all samples had a RIN above 8. The library was prepared using 500 ng of total RNA with the KAPA mRNAseq stranded kit (KAPA, Cat no. KK8420). Ligation was performed with 9 nM final concentration of Illumina index and 10 PCR cycles were required to amplify cDNA libraries. The libraries were quantified using QuBit and BioAnalyzer, diluted to 10 nM and normalized by qPCR using the KAPA library quantification kit (KAPA; Cat no. KK4973). The libraries were then pooled to equimolar concentration before their sequencing with the Illumina Hiseq2000 using the Hiseq Reagent Kit v3 (200 cycles, paired-end) and 1.7 nM of the pooled library. Around 40 M paired-end PF reads were generated per sample and used for bioinformatic analysis. This process follows the protocol published by Abusarah et al.[11] Library preparation and sequencing was performed at the Institute for Research in Immunology and Cancer (IRIC)'s Genomics Platform.

Bioinformatics analysis

Estimated mRNA sequencing reads derived from wild-type C57BL/6 mice BM-derived DCs were extracted from GEO accession number GSE158783. For MSCs and IRMs comparison, mRNA sequencing, downstream analyses and generation of the count matrix have been described elsewhere.[11] Briefly, the two datasets were merged using quantile normalization followed by a log transformation of the dataset, and subsequent differential gene expression analysis was performed using the Bayesian approach as implemented in the limma R package.[73] Gene set enrichment analysis was performed on the ranked list of genes as described previously.[11,74] All plots were created in R from custom scripts and the ClusterProfiler package.[75] If not mentioned in the text, a log2 fold change >1 and a False discovery rate <0.05 were set as significance cutoffs. Pattern matching (aka connectivity score) was conducted to assess how likely two transcriptional signatures are similar. To this end, the top 250 up-/250 down-regulated genes from the DC signature were scored against the ranked list of differentially expressed genes in IRMs. The combined p-value from both up and down signatures were calculated using a Fisher test. The enrichment score (ESup - ESdown)/2 was obtained after 10,000 random permutations (Smirnov et al., 2016). Overrepresentation of GO biological processes was conducted with a hypergeometric test in ClusterProfiler at a false discovery threshold of 5%

Statistical analysis

Depending on the study, p-values were calculated using the student's t-test, one-way analysis of variance (ANOVA) or the log rank test using GraphPad Prism. Results are represented as means with standard deviation (S.D.) error bars, and statistical significance is represented with asterisks: *P<0.05, **P<0.01, ***P<0.001.